AD_____

Award Number: W81XWH-06-1-0484

TITLE: Simulations to Evaluate Accuracy and Patient Dose in Neutron-Stimulated, Emission-Computed Tomography (NSECT) for Diagnosis of Breast Cancer

PRINCIPAL INVESTIGATOR: Anuj J. Kapadia

CONTRACTING ORGANIZATION: Duke University
Durham, NC 27708

REPORT DATE: April 2007

TYPE OF REPORT: Annual Summary

PREPARED FOR: U.S. Army Medical Research and Materiel Command
Fort Detrick, Maryland 21702-5012

# REPORT DOCUMENTATION PAGE

*Form Approved*
*OMB No. 0704-0188*



| 1. REPORT DATE | 2. REPORT TYPE | 3. DATES COVERED |
|---|---|---|
| 01-04-2007 | Annual Summary | 31 Mar 2006 – 30 Mar 2007 |

**4. TITLE AND SUBTITLE**

Simulations to Evaluate Accuracy and Patient Dose in Neutron-Stimulated, Emission-Computed Tomography (NSECT) for Diagnosis of Breast Cancer

**5a. CONTRACT NUMBER**

**5b. GRANT NUMBER**
W81XWH-06-1-0484

**5c. PROGRAM ELEMENT NUMBER**

**6. AUTHOR(S)**

Anuj J. Kapadia

Email: anuj.kapadia@duke.edu

**5d. PROJECT NUMBER**

**5e. TASK NUMBER**

**5f. WORK UNIT NUMBER**

**7. PERFORMING ORGANIZATION NAME(S) AND ADDRESS(ES)**

Duke University
Durham, NC 27708

**8. PERFORMING ORGANIZATION REPORT NUMBER**

**9. SPONSORING / MONITORING AGENCY NAME(S) AND ADDRESS(ES)**
U.S. Army Medical Research and Materiel Command
Fort Detrick, Maryland 21702-5012

**10. SPONSOR/MONITOR'S ACRONYM(S)**

**11. SPONSOR/MONITOR'S REPORT NUMBER(S)**

**12. DISTRIBUTION / AVAILABILITY STATEMENT**
Approved for Public Release; Distribution Unlimited

**13. SUPPLEMENTARY NOTES**
Original contains colored plates: ALL DTIC reproductions will be in black and white.

**14. ABSTRACT**

We are developing a tomographic technique called Neutron Stimulated Emission Computed Tomography (NSECT) for early detection of breast cancer. NSECT is sensitive to metabolic changes in trace element concentrations that are seen in tumors at very early stages of development. Detecting and measuring these element concentrations has the potential to detect breast cancer early. Using neutrons as the imaging radiation leads to significant concerns about patient dose. While preliminary experiments show that it is possible to perform NSECT scans with dose similar to that of an abdominal CT scan, one of our primary goals in this project is to reduce dose further to allow NSECT to be more easily accepted as a screening tool. This project aims at evaluating the effects of NSECT dose-reduction techniques on the accuracy of cancer diagnosis. There are 4 dose reduction techniques under evaluation: reducing neutron flux; using fewer spatial projections; fewer angles; and using multiple detectors. As evaluation of each technique individually using experimental studies is not feasible, this study uses Monte-Carlo simulations as an alternative. In the first part of the study, we have designed and built a Monte Carlo simulation of the NSECT tomographic scanning system using GEANT4. We have designed the scanning system as a 3 part system consisting of: (a) a neutron beam source with user-defined neutron flux and neutron beam width, (b) a gantry with user-defined spatial and angular beam sampling rates, and (c) gamma detectors with user-defined detector material, radius, efficiency and location. We have also built GEANT4 phantoms for benign and malignant breast tissue based on element concentrations reported in various experimental studies. Finally, we have integrated the phantoms and tomographic system to simulate a complete NSECT scan of the human breast.

**15. SUBJECT TERMS**
Neutron, spectroscopy, NSECT, breast, tomography, imaging, MLEM, Monte Carlo simulation, Geant4.

| 16. SECURITY CLASSIFICATION OF: | | | 17. LIMITATION OF ABSTRACT | 18. NUMBER OF PAGES | 19a. NAME OF RESPONSIBLE PERSON |
|---|---|---|---|---|---|
| a. REPORT | b. ABSTRACT | c. THIS PAGE | | | USAMRMC |
| U | U | U | UU | 42 | 19b. TELEPHONE NUMBER *(include area code)* |

## Table of Contents

**Page**

## INTRODUCTION

Breast cancer is the leading type of cancer to affect women all over the world. In the United States alone, breast cancer is expected to account for 32% of all new cancer cases among women. The American Cancer Society has estimated that 180,510 new cases of breast cancer will be detected in 2007, and 40,910 of these will result in death [1]. Early detection has proved to be the most effective technique to increase survival rates for this disease. Screening x-ray mammography is presently the only FDA approved screening tool for early detection of breast cancer. While it has proved to be effective, screening mammography has several limitations in trying to detect masses and spiculations in mammograms. First, it requires that the mammograms have good contrast, which is often difficult to achieve in women with dense breasts. Second, it uses an anatomic approach in trying to identify abnormalities in mammograms, making it essential that the abnormality be developed enough to show masses and calcifications clearly. This development usually comes at advanced stages of tumor growth. Finally, it has limitations in classifying detected abnormalities as benign or malignant. Several artificial intelligence tools, developed to classify detected lesions as benign or malignant have been investigated, but none have been FDA approved yet. These tools, such as computer aided diagnosis (not to be confused with the FDA approved computer aided detection systems now available), make their decisions based on morphological features such as shape, size, texture, etc. While they are fairly effective in classifying a detected lesion as benign or malignant, their dependence on analyzing an already visible lesion reduces their decision-making ability for lesions in very early stages of development.

To overcome these limitations, we are developing a technique that is sensitive to metabolic changes seen in malignant tumors during very early developmental stages. Various experiments conducted on trace elements in the human body have shown that malignant tumors exhibit changes in trace elements concentrations during early stages of development [2-7]. Quantifying these element concentrations, such as those of rubidium, cesium, aluminum and antimony, could potentially enable diagnosis of breast cancer at very early stages much before the tumor grows large enough to be detected by existing imaging techniques.

### Principle

Our technique, called Neutron Stimulated Emission Computed Tomography (NSECT), uses a spectroscopic approach to analyze changes in element concentrations at molecular levels in breast tissue [8, 9]. NSECT analyzes spectral information obtained from inelastic scattering between a neutron and a target atomic nucleus to identify the atom and determine its concentration in the tissue. Neutrons striking a stable atomic nucleus stimulate it to emit gamma radiation which is unique to that element. Measuring the energy and quantity of the emitted radiation allows direct determining of the emitting element concentration. Ratios of trace element concentrations detected can then be used to classify the tissue as benign or malignant. Our preliminary data suggests that this technique has great potential in developing into an effective screening tool for early diagnosis of breast cancer.

Using neutrons as the imaging radiation leads to significant concerns about patient dose. At the energies we propose, neutrons are known to damage the body 10 times more than x-rays. Reducing patient dose is a critical task in making NSECT feasible as a diagnostic technique for breast cancer. Our preliminary experiments show that it is possible to achieve an effective patient dose of about 15 mSv, which is comparable to the typical dose from an abdominal CT scan. This is possible because though individual neutrons cause more tissue damage than x-rays, it takes an immensely smaller number of neutrons to create an NSECT image, than x-rays to create a CT image. A primary objective of this project is to reduce dose further to allow NSECT to be more easily accepted as a screening tool.

Reducing patient dose in NSECT will be accompanied by a reduction in detection accuracy. This project aims at evaluating the trade-offs between patient dose and accuracy in NSECT, for 4 proposed dose-reduction techniques, and determine the minimal values of patient dose for which accuracy in the system remains high enough to effectively diagnose breast cancer.

The 4 different techniques proposed for dose-reduction in NSECT are a) neutron flux reduction, b) reduction in projection spatial sampling, c) reduction in angular sampling (fewer angles), and d) using multiple detectors. The first 3 techniques will reduce dose by reducing the amount of radiation incident on the body, while using multiple detectors will extract maximum information from the incident radiation. It is very difficult to evaluate the effects of each of these techniques individually using experimental NSECT studies, as these studies, which are at present performed in a nuclear accelerator lab, are prohibitively time consuming. We propose to approach this experiment using Monte-Carlo simulations as an alternative.

## BODY

**Task 1: Build a Monte Carlo simulation of the tomographic scanning system using GEANT4**
(Months 1-10)

a) Simulate neutron beam source with user-defined neutron flux and neutron beam width
b) Simulate gantry with user-defined spatial and angular beam sampling rates
c) Simulate 2 types of gamma detectors under consideration with user-defined radius, efficiency and location: bismuth germanate (BGO), and high-purity germanium (HPGe)

**Status:** This task has been completed exactly as proposed.

The first task of this project is to develop a simulation tool to model the interactions between incoming neutrons and atomic nuclei as a practical alternative to evaluate the effects of dose-reduction techniques on detection accuracy. This is performed using stochastic modeling methods in GEANT4, a high-energy-physics object-oriented Monte-Carlo programming toolkit for simulating the passage of particles through matter. Developed by a worldwide collaboration of about 100 scientists in Europe, Russia, Japan, Canada and the United States, GEANT4 accounts for all the diverse interactions of particles with matter across a wide energy range. It incorporates a powerful set of random number generators, physics units and constants, and provides all the tools required for detector simulation, including geometry, tracking, detector response management, visualization and user interface. Its programming package allows individual simulation of different types of user-defined “objects” such as neutron sources and detectors composed of a single element or a mixture of elements, which can be integrated into a single module separately through its object-oriented nature.

**Preliminary experimental model:** The simulation is based on the experimental model, which works as follows. A neutron, incident on a body, travels freely along its projected path until it collides with an atomic nucleus. If the neutron scatters inelastically with a target atomic nucleus, the nucleus gets excited into one of its quantized, higher-energy states. This excited nucleus then rapidly decays to a lower state, emitting a gamma ray photon, whose energy is equal to the difference between the two states. These non-overlapping energy states are well established and unique to each element and isotope. Detection and analysis of the emitted gamma ray spectrum enables identification of the target atom. An energy-sensitive gamma detector is used to capture the emitted gamma photons. Tomography is performed using the translate-rotate configuration, as in first generation CT scanners, by translating the beam horizontally through the entire sample length, then rotating the beam through a fixed angle and repeating the process. Tomographic reconstruction of these scanned projections yields a two-dimensional slice of element concentration and distribution in the sample. The translate-rotate geometry is appropriate for initial proof of concept studies using phantom, specimen or small animals. Once feasibility is demonstrated, other geometries can be used in future clinical systems.

**Simulated Model:** The simulated model consists of 4 parts – (a) World, (b) Neutron Source, (c) Tomographic Gantry, and (d) Gamma Detectors. Each part has been designed as a separate Geant4 object to facilitate modifying individual parameters on one object independently of the others.

(a) **World:** Geant4 requires creation of a finite virtual space called the 'world', which acts as the world for the experiment. This world defines the virtual space within which the experiment will occur. All sources, detectors and samples are placed in the world. Particle interactions are tracked only as long as they occur in this world, and particles exiting the world are considered spent events. For this study, the world was defined as a cube with edge 1m, and filled with air.

(b) **Neutron Source:** The neutron source is created by defining a 'Geant4 Particle Gun', with user defined options for particle type and energy. For breast studies, the incident particles are set to 2.5 MeV neutrons. The gun is placed at the left edge of the world so that every particle exiting the gun enters directly into the world to form a neutron beam. The exit position of the particle from the gun is given a user-defined width, which determines the width of the emitted neutron beam. GEANT4 processes each neutron as an individual event instead of a beam. Hence to create a beam with a finite width, a random number generator is used to select the point of emission of the individual neutron within a certain distance about the center of the gun. This distance about the gun center forms the beam width of the emitted neutron beam. For this experiment, the beam-width was set at 1cm. The result of the GEANT4 'source' object is a collection of individual neutron events distributed randomly within a 1cm width about the gun-center, forming a 2.5 MeV neutron beam with a 1cm user-defined width.

(c) **Tomographic Gantry:** Tomography in NSECT is currently performed in a manner similar to first generation CT with a stationary beam and single element detector. The phantom is translated through the beam, then rotated through a finite angle and translated through the beam again. In the simulation, this translation-rotation is facilitated by the tomographic gantry. The tomographic gantry is designed by creating a gantry chamber within the world, filling it with the same material as the world (air), and placing it in the center of the world. The chamber can be rotated to any angle from 0-180 degrees in clockwise or anticlockwise direction, and can be moved to any desired xyz lateral position within the world. The user defines the number of translation and rotation positions along with the translation and rotation increments. Once a phantom is created, it can simply be placed inside this gantry chamber, and the sample can then be rotated and translated along with the gantry using gantry parameters. Typical values for rotation and translation in breast study experiments are 15 lateral steps at 7mm intervals and 8 angles at 22.5 degree intervals.

(d) **Gamma Detectors:** Gamma detectors are created as solid cylinders with user-defined diameter and height. Each cylinder is filled with one of 2 detector materials:

(i) High-purity germanium, HPGe (density= 5.32 g/cm$^3$)

(ii) Bismuth Germanate, BGO (density= 7.13 g/cm$^3$, 67.1% Bi, 17.5% Ge, and 15.4% O).

The detector material is 'sensitized', i.e. defined to track particle interactions and record the energy deposited at each interaction. The detector can be placed at any location in the world. In the current configuration, the detector is modeled as a 9cm diameter cylinder with 8cm height, similar to the detectors used in the physical NSECT experiments. The detector is placed at a backward angle of 135 degrees in the beam plane, mimicking the position of the detector in the physical experiment where a backward angle is used to minimize damage to the detector from forward scattered neutrons. Detector efficiency is modeled by collecting information from all events occurring in the detector and then retaining only a required fraction of these events. For example, for a 60% efficient HPGe detector, 100% of events will be recorded, but only 60% of these will be used to generate spectral results.

Fig.1 shows and example of this geometry with the world housing the gamma detectors and the phantom. The target gantry is an invisible box around the ellipsoid breast phantom. The gun is an invisible source at the left edge of the figure, emitting neutrons (shown in blue) that illuminate the breast.

**Task 2: Build GEANT4 phantoms for benign and malignant breast tissue based on element concentrations reported in various experimental studies.** (Months 11-12)

**Status:** This task has been completed as proposed.

This task aims at designing Geant4 phantoms of the benign and malignant breast, which will be scanned using the simulated NSECT system. Two sets of phantoms are designed for this study – (a) Breast Phantom (b) Dose Phantom.

(a) **Breast Phantom:** Breast phantoms are simulated in GEANT4 as ellipsoids of 10cm x 6 cm x 5cm height. The phantom is filled with benign or malignant breast tissue, which is classified on the basis of its elemental composition as shown in table 1 below. Apart from the regular elements found in human breast tissue, i.e. hydrogen, oxygen, carbon and nitrogen, the breast tissue models are given trace elements in concentrations corresponding to benign and malignant breast tissue as reported in [2-6, 10]. The density of breast tissue was defined as 0.93 g/cm$^3$.

| | **Normal (%)** | **Malignant (%)** |
|---|---|---|
| **Oxygen** | 61.429 | 61.429 |
| **Carbon** | 22.857 | 22.857 |
| **Hydrogen** | 12.649 | 12.510 |
| **Nitrogen** | 2.571 | 2.571 |
| **Chlorine** | 1.98E-2 | 2.15E-2 |
| **Sodium** | 1.85E-2 | 2E-2 |
| **Potassium** | 8.94E-2 | 1.96E-2 |
| **Iron** | 9.8E-3 | 7.85E-3 |
| **Calcium** | 8.29E-3 | 1.13E-2 |
| **Zinc** | 1.17E-3 | 1.14E-3 |
| **Bromine** | 7.07E-4 | 6.55E-4 |
| **Aluminum** | 6.67E-4 | 5.7E-4 |
| **Rubidium** | 5.98E-4 | 5.84E-4 |
| **Manganese** | 3.88E-5 | 3.16E-5 |
| **Cobalt** | 2.06E-5 | 1.98E-5 |
| **Cesium** | 3.27E-7 | 3.6E-7 |

Table 1: Breast tissue composition for normal and malignant models (from [11]).
The percentages were calculated by first converting dry weights to wet weights.

(b) **Dose Phantom:** A separate phantom of the torso is designed to perform dose measurements. This phantom consists of the whole torso including the breast, and accounts for the larger anatomic structures encountered by a neutron beam when scanning a patient. The torso is modeled as a larger ellipsoid, 40cm x 30cm x 30 cm height, similar to a human torso. The breasts are modeled as hemispheres located on one edge of the torso. As neutron dose depends primarily on the hydrogen content of tissue, the torso and breast regions are both filled with water to

approximate the hydrogen content of the body. This phantom is sensitized to measure the energy deposited in it, which can then be converted to an absorbed dose equivalent. As energy measurements are made within the phantom, separate gamma detectors are not required.

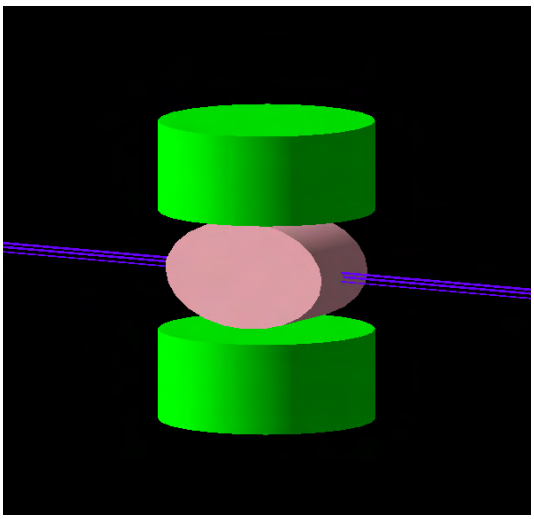

Fig 1. Breast phantom flanked by gamma detectors on either side. The black region represents the world, the pink region is the breast, and green cylinders correspond to gamma detectors. Neutrons passing through the breast are shown in blue.

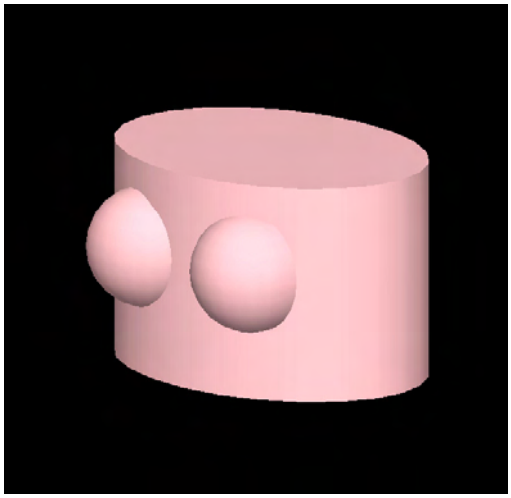

Fig 2. Dose phantom showing the torso and the relative position of the breasts. For dose estimation simulations, the torso and breasts are all filled with water. As dose is calculated by measuring the energy deposited in the torso and breasts, gamma detectors are not required.

**Task 3: Integrate simulations built in tasks 1 and 2 into a single module to allow simulation of a complete NSECT patient scan from patient irradiation to spectrum acquisition.** (Months 11-12)

**Status:** Completed as proposed.

Geant4 is an object oriented programming package, which allows creation of each part as an individual object. This task integrates all the objects to create a complete simulation of the NSECT acquisition system. The phantoms created in Task 2 are integrated with the gantry created in Task 1. While Geant4 contains libraries for a large number of high-energy physics interactions for a host of particles, it is left to the user to select which interactions to model for each application.

**Task 4: Determine element concentrations from simulated gamma spectra using spectral analysis and compare with pre-defined concentration levels in simulated phantom.** Months (13-15)

**Status:** This task is currently under way.

Spectral data is currently being generated from the breast phantom simulations built in tasks 1-3. Preliminary versions of algorithms for spectral analysis have been built and tested using experimental spectrums from nuclear laboratory experiments [11]. These algorithms will be refined with the use of simulated data from this task.

**Task 5: Reconstruct tomographic images using MLEM reconstruction algorithms.** (Months 16-20)

**Status:** This task is currently under way.

A preliminary version of the MLEM reconstruction algorithm has been built and tested with experimental data from nuclear laboratory experiments [12]. This preliminary version is a direct implementation of Lange and Carson's algorithm for emission tomography with Poisson counting [13]. The algorithm will be tested and refined using the simulation data generated in task 4.

## KEY RESEARCH ACCOMPLISHMENTS

- The entire NSECT acquisition system has been simulated using the Geant4 environment, which makes it possible to continue system evaluation and development without requiring a neutron beam.
- Two types of gamma detectors have been designed in the simulation environment, which makes it possible to evaluate the option of using a larger number of low-cost low-resolution detectors to achieve the required accuracy.
- Phantoms for benign and malignant breast tissue have been designed and implemented in the Geant4 environment.
- Spectral data has been obtained from benign and malignant breast biopsy specimens, for validation of the Geant4 simulations.

## REPORTABLE OUTCOMES

The following conference proceedings and manuscripts have been attached in the appendix section.

1. **Kapadia AJ**, Sharma AC, Tourassi GD, Bender JE, Howell CR, Crowell AS, Kiser MR, and Floyd CE, "Non-Invasive Estimation of Potassium (39K) in Bovine Liver Using Neutron Stimulated Emission Computed Tomography (NSECT)," *Proceedings of IEEE Nuclear Science Symposium, Medical Imaging Conference 2006*.

2. **Kapadia AJ**, Sharma AC, Tourassi GD, Bender JE, Howell CR, Crowell AS, Kiser MR, and Floyd CE, "Neutron Stimulated Emission Computed Tomography (NSECT) for Early Detection of Breast Cancer," *Proceedings of IEEE Nuclear Science Symposium, Medical Imaging Conference 2006*.

3. **Kapadia AJ**, Sharma AC, Tourassi GD, Bender JE, Howell CR, Crowell AS, Kiser MR, and Floyd CE, "Neutron Spectroscopy of Mouse Using Neutron Stimulated Emission Computed Tomography (NSECT)," *Proceedings of IEEE Nuclear Science Symposium, Medical Imaging Conference 2006*.

4. **Kapadia AJ,** Sharma AC, Bender JE, Tourassi GD, Howell CR, Crowell AS, Kiser MR, Harrawood BP, and Floyd CE, "Neutron Stimulated Emission Computed Tomography for Diagnosis of Breast Cancer," *IEEE Trans Nuc Sci (submitted)*, 2007.

5. Bender JE, **Kapadia AJ,** Sharma AC, Tourassi GD, Harrawood BP, and Floyd CE, "Breast cancer detection using Neutron Stimulated Emission Computed Tomography: prominent elements and dose requirements," *Medical Phyiscs, (submitted)*, 2007.

## CONCLUSION

We have simulated the NSECT acquisition system using the Geant4 Monte Carlo simulation environment. This will allow further development and system evaluation using easily accessible computing resources. Future work will focus on generating spectrums from the breast phantoms and evaluate the trade-off between accuracy as patient dose is reduced.

## REFERENCES


[1] ACS, "Cancer Facts and Figures 2007," American Cancer Society, Atlanta 2007 2006.

[2] Garg A, V. Singh, et al., "An elemental correlation study in cancerous and normal breast tissue with successive clinical stages by neutron activation analysis," *Biological Trace Element Research*, vol. 46, pp. 185-202, 1994.

[3] Mussalo-Rauhamaa H, Piepponen S, Lehto J, Kauppila R, and Auvinen O, "Cu, Zn, Se and Mg concentrations in breast fat of Finnish breast cancer patients and healthy controls," *Trace Elements in Medicine*, vol. 10, pp. 13-15, 1993.

[4] Ng K-H, Bradley D, and Looi L-M, "Elevated trace element concentrations in malignant breast tissues," *British Journal of Radiology*, vol. 70, pp. 375-382, 1997.

[5] Ng K-H, Ong S-H, Bradley DA, and Looi L-M, "Discriminant analysis of normal and malignant breast tissue based upon INAA investigation of elemental concentration," *Appl. Radiat. Isot.*, vol. 48, pp. 105-109, 1997.

[6] Rizk S and Sky-Peck H, "Comparison between concentrations of trace elements in normal and neoplastic human breast tissue," *Cancer Research*, vol. 44, pp. 5390-5394, 1984.

[7] Yaman M, Atici D, Bakirdere S, and Akdeniz I, "Comparison of trace metal concentrations in malign and benign human prostate," *J. Med. Chem.*, vol. 48, pp. 630-634, 2005.

[8] Floyd CE, Bender JE, Sharma AC, Kapadia AJ, Xia JQ, Harrawood BP, Tourassi GD, Lo JY, Crowell AS, and Howell CR, "Introduction to neutron stimulated emission computed tomography," *Physics in Medicine and Biology*, vol. 51, pp. 3375-3390, 2006.

[9] Floyd CE, Howell CR, Harrawood BP, Crowell AS, Kapadia AJ, Macri R, Xia JQ, Pedroni R, Bowsher J, Kiser MR, Tourassi GD, Tornow W, and Walter R, "Neutron Stimulated Emission Computed Tomography of Stable Isotopes," *Proceedings of SPIE Medical Imaging 2004*, vol. 5368, pp. 248-254.

[10] Schwartz A and Fink R, "Trace Elements in Normal and Malignant Human Breast Tissue," *Surgery*, vol. 76, pp. 325-329, 1974.

[11] Bender JE, Kapadia AJ, Sharma AC, Tourassi GD, Harrawood BP, and Floyd CE, "Breast cancer detection using Neutron Stimulated Emission Computed Tomography: prominent elements and dose requirements," *Medical Phyiscs*, (submitted), 2007.

[12] Floyd CE, Kapadia AJ, Bender JE, Sharma AC, Xia JQ, Harrawood BP, Tourassi GD, Lo JY, Crowell AS, and Howell CR, "Neutron Stimulated Emission Computed Tomography of a Multi-Element Phantom," *IEEE Trans Med Imag (submitted)*, 2006.

[13] Lange K and Carson R, "EM reconstruction Algorithms for Emission and Transmission Tomography," *Journal of Computer Assisted Tomography*, vol. 8, pp. 306-316, 1984.

**APPENDICES**

# Neutron Stimulated Emission Computed Tomography (NSECT) for Early Detection of Breast Cancer

Anuj J. Kapadia, Amy C. Sharma, Georgia D. Tourassi, Janelle E. Bender, Alexander S. Crowell, Matthew R. Kiser, Calvin R. Howell, Carey E. Floyd Jr.

***Abstract*– Neutron stimulated emission computed tomography (NSECT) is being developed as a non-invasive spectroscopic technique to determine element concentrations in the human body. We have implemented an NSECT system that uses a beam of high-energy neutrons to identify element concentrations in tissue and create 2-dimensional maps of elemental distribution through a single non-invasive tomographic scan. Neutrons scatter inelastically with atomic nuclei in tissue, causing them to emit characteristic gamma photons. These gamma photons are detected and identified using an energy-sensitive gamma detector. By measuring the energy and number of emitted gamma photons, the system can determine the elemental composition of the target tissue. NSECT has the advantage of being able to detect breast cancer at very early stages compared to anatomic screening techniques, as it detects changes in trace element concentrations in the breast, which usually occur before anatomical features such as tumors and micro-calcifications appear. The tomographic scanning system eliminates the need for breast compression and patient disrobing. The system design can be made portable by using a commercially available portable neutron source with a gamma detector. From our preliminary results, NSECT shows significant promise in early diagnosis of breast cancer. It has the potential to evolve into an easily accessible screening modality and diagnostic technique for breast cancer, which can detect and identify malignant tissue in the breast and generate a two-dimensional image through a single non-invasive tomographic scan. Patient dose levels from NSECT are comparable to those of screening mammography. Efforts are under way to achieve the micro-gram sensitivity required for in-vivo trace element detection in the breast at the lowest possible patient dose levels. Our final goal is to implement a portable, low-dose tomographic screening system for breast cancer which does not require breast compression or invasive biopsies.**

Manuscript received November 13, 2006. This work was supported by the NIH/NCI grant 1-R21-CA106873-01 and in part by Department of Defense (Breast Cancer Research Program) under award number W81XWH-06-1-0484.

A. J. Kapadia is with the Department of Biomedical Engineering and the Duke Advanced Imaging Laboratories (DAILabs) of the Department of Radiology, Duke University, Durham, NC 27710, USA (phone: 919-684-1470; fax: 919-684-1491; email: anuj.kapadia@duke.edu).

A.C. Sharma is with the Department of Biomedical Engineering and the DAILabs of the Department of Radiology, Duke University, Durham, NC 27710, USA (phone: 919-684-1471; fax: 919-684-1491; email: anc4@duke.edu).

G.D. Tourassi is with the DAILabs of the Department of Radiology, Duke University, Durham, NC 27710, USA (phone: 919-684-1447; fax: 919-684-1491; email: gt@deckard.duhs.duke.edu).

J. E. Bender is with the Department of Biomedical Engineering, Duke University, Durham, NC 27710, USA (email: janelle.bender@duke.edu).

A. S. Crowell is with the Department of Physics, Duke University and the Triangle Universities Nuclear Laboratory, Durham, NC 27708, USA (phone: 919-660-2639; fax: 919-660-2634; email: crowell@tunl.duke.edu).

M. R. Kiser is with the Department of Physics, Duke University and the Triangle Universities Nuclear Laboratory, Durham, NC 27708, USA (phone: 919-660-2639; fax: 919-660-2634; email: kiser@tunl.duke.edu).

C. R. Howell is with the Department of Physics, Duke University and the Triangle Universities Nuclear Laboratory, Durham, NC 27708, USA (phone: 919-660-2632; fax: 919-660-2634; email: howell@tunl.duke.edu).

C. E. Floyd Jr. is with the DAILabs of the Department of Radiology, Duke University Medical Center and the Department of Biomedical Engineering Duke University, Durham, NC 27710.

## I. Introduction

Neutron stimulated emission computed tomography (NSECT) is being developed as a non-invasive spectroscopic technique to determine element concentrations in the human body. We have implemented and demonstrated the feasibility of an NSECT system that uses a beam of high-energy fast neutrons to identify element concentrations in tissue and create 2-dimensional maps of elemental distribution in the tissue, all through a single non-invasive tomographic scan [1, 2]. NSECT relies on inelastic scattering interactions between neutrons and target atomic nuclei to obtain this information. If a neutron incident on tissue scatters inelastically with an atomic nucleus in the target tissue, it excites the nucleus to a higher energy state that is often unstable and short-lived. The unstable nucleus then rapidly decays to its ground state from the higher energy state, emitting the excess energy as a gamma photon. The energy of the emitted photon is equal to the energy difference between the two states, and can be measured by an energy-sensitive gamma detector. As these energy states and transitions are mostly unique to each element and isotope, an atom can be identified by measuring the energy of the emitted gamma photon.

## II. Relevance

Non-invasive quantification of elements in the body shows great potential in diagnosis of several disorders that are characterized by changes in element concentration in the affected organ or tissue. One of these disorders is breast cancer. Several studies have shown that a change in trace element concentration is often associated with cancer, specifically in the breast [3-10], prostate [11] and brain [12, 13]. Breast cancer has been associated with changes in Al, Br, Ca, Cl, Co, Cs, Cu, Fe, K, Mn, Na, Rb, Sb, Se, Zn; prostate cancer with Ca, Cu, Fe, Mg, Ni, Zn; and brain cancer with B, Ba, Sr, Zn. In many cancers, these element concentration changes are seen much before morphologic changes such as

tumors and micro-calcifications develop to a point where they can be detected by current imaging modalities. Quantifying these element concentrations could enable in-vivo cancer diagnosis earlier than is possible with conventional imaging techniques, potentially increasing survival rates of patients through early diagnosis.

Additionally, disorders such as hemochromatosis (liver iron overload associated with thalassemia and sickle cell anemia) and Wilson's disease (liver copper overload), are characterized by increased iron and copper concentration respectively in the liver [14, 15]. These are currently diagnosed through liver biopsy, which is an unpleasant procedure that has several complications associated with it [16, 17]. NSECT has the potential to diagnose liver overload disorders through a non-invasive scan with a dose level equivalent to that of a single abdominal CT scan.

## III. Methods

NSECT experiments are performed at the Triangle Universities Nuclear Laboratory (TUNL) accelerator lab, on Duke University's campus. Their shielded neutron source is an excellent source of fast neutrons (energy in MeV range) with adequate high-flux beams, which can be collimated to desired size and shape using swappable collimator inserts. A brief description of the experimental setup follows.

### A. Experimental Setup

A 5 MeV neutron beam is produced through a $^{2}H(d,n)^{3}He$ reaction, by bombarding a deuterium gas target with a deuteron beam accelerated by a Van de Graaf accelerator. This beam is collimated to a desired profile and size using appropriate copper collimators, and focused onto the target tissue sample. Neutron flux at the target is monitored by a plastic scintillator attached to a photo-multiplier tube placed between the collimator and the target. The target tissue sample is placed on a translation-rotation stage, which enables tomography through a first generation CT scanning technique. The sample is first translated through a fixed number of steps, then rotated through a fixed angular rotation and translated again. This process is repeated for the required number of angles. Gamma photons emitted by the sample are counted by high purity germanium detectors (HPGe) hooked up to a data acquisition system. These detectors are shielded from unwanted neutrons and gammas using lead and borated paraffin wax shielding.

### B. Patient Dose

Using neutrons as the incident radiation leads to significant concerns about patient dose. At the energies we propose, neutrons are known to damage the body 10 times more than x-rays. However, as it takes an immensely smaller number of neutrons to create an NSECT image than x-rays required to create a mammogram, it is possible to achieve dose levels comparable to other ionizing radiation modalities. Our preliminary experiments suggest that for breast cancer detection, it may be possible to achieve effective patient dose levels of approximately 15 mSv. By increasing the number of detectors and using high-flux neutron sources to reduce scan time, dose levels can potentially be brought down to values comparable to screening mammography.

Dose measurements are currently done through a Geant4 simulation which models the acquisition geometry, neutron beam characteristics and sample data. The energy deposited in the sample is counted and used to calculate an effective dose equivalent for the organ.

### C. Current Status

Several samples have been scanned to date, ranging from solid metals for calibration and sensitivity studies, to biological samples such as excised breast tissue, bovine liver and a fixed mouse specimen. These spectra have been shown below. We have also successfully reconstructed a 2-dimensional image from a tomographic scan of a mixed iron and copper sample and separately identified and reconstructed each element in the sample [18].

### D. Background Correction

Background correction is generally performed using three techniques. First, time-of-flight correction is used to reduce time-uncorrelated background noise from random sources of activity in the beam room. Using a pulsed deuteron beam, it is possible to calculate the expected arrival time of gamma photons originating from the sample through neutron inelastic scatter. Events that occur outside this expected arrival time window are discarded as noise events and suppressed.

Second, sample-related background is reduced by acquiring and subtracting a sample out scan from the sample spectrum. For solid metal samples, the sample-out scan is generally acquired with room air in place of the metal. For biological tissue, a sample of distilled water of equal mass as the scanned tissue is used to generate elastic neutron scatter comparable to that of the original tissue. Hydrogen nuclei in water (which is a large component of biological tissue) have the same mass as neutrons. Hence, a lot of neutron scatter is generated while scanning a tissue sample. Scattered neutrons can interact with other materials in the room and generate inelastic scatter gamma photons from them. The sample-out scan is used to estimate this background and subtract it from the sample in spectrum.

Finally, the residual underlying background, which is an effect of the detector efficiency, is modeled and subtracted using a polynomial curve fit. A detected photon may not deposit all of its energy in a single step. Instead it may do so in several steps in the detector crystal, causing an energy spread over the lower channels of the detector. As a result, there is a gradual increase in photon counts over the lower detector channels. This extra-count trend is fitted using a polynomial curve fit and subtracted from the spectrum.

## IV. Results

Background corrected spectrums obtained from several samples are shown here. Fig. 1 shows a spectrum from a

mixture of iron, potassium, sodium and chlorine in water. As can be seen from the spectrum, peaks corresponding to Fe, Cl, Na and K are easily distinguished from each other.

Fig. 2 shows a spectrum from bovine liver. Several elements present in the liver were identified and their concentrations were determined. The presence of some elements was cross-validated through a quantitative neutron activation analysis scan of the liver sample. The concentrations predicted by NSECT differed from the NAA values by 15-50% for different elements.

Fig. 3 shows a spectrum from a fixed mouse specimen. Peaks can be seen for carbon and calcium from bone and tissue respectively. Also seen are peaks for germanium from the detectors and gadolinium from the fixing solution.

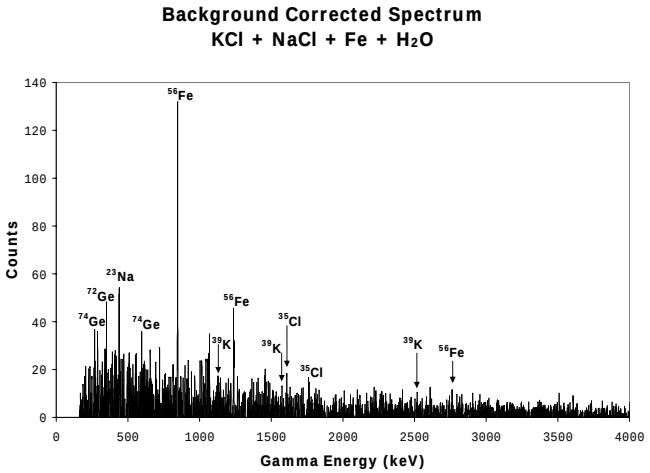


Fig.1. Gamma spectrum from a KCl, NaCl and Fe solution in water showing peaks corresponding to excited states in $^{39}$K, $^{23}$Na, $^{35}$Cl, $^{37}$Cl, $^{56}$Fe, $^{70}$Ge, and $^{74}$Ge. These spectra are shown without neutron or gamma attenuation correction.

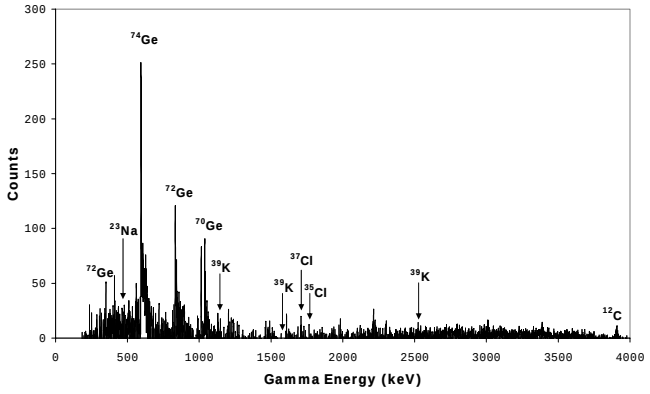


Fig.2. Gamma spectrum from a bovine liver specimen showing peaks corresponding to excited states in $^{39}$K, $^{23}$Na, $^{35}$Cl, $^{37}$Cl, $^{56}$Fe, $^{70}$Ge, and $^{74}$Ge Gamma peaks are also seen for $^{12}$C (escape peaks) from tissue. These spectra are shown without neutron or gamma attenuation correction.

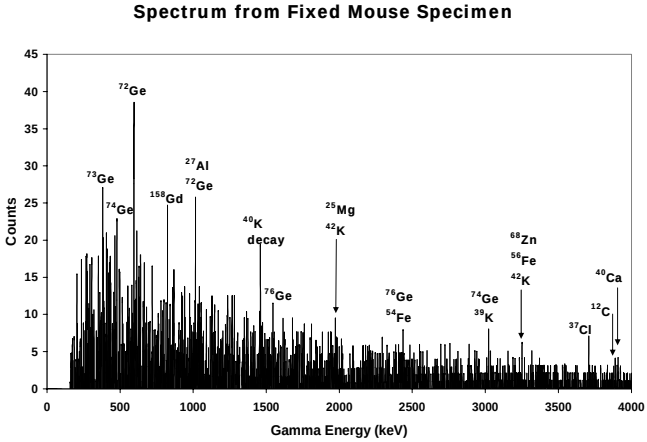


Fig.3. Gamma spectrum from a formalin fixed mouse specimen showing peaks corresponding to excited states in various elements. Gamma peaks are seen for $^{12}$C (escape peaks), $^{40}$Ca, $^{39}$K, $^{27}$Al, $^{37}$Cl, $^{56}$Fe, $^{68}$Zn and $^{25}$Mg. Gamma peaks are also seen for $^{72}$Ge and $^{74}$Ge from the germanium detector, and $^{158}$Gd and $^{160}$Gd from the fixing solution. Peaks with multiple potential element matches are labeled accordingly. These spectra are shown without neutron or gamma attenuation correction.

## V. Conclusion and Future Work

NSECT shows significant promise in early diagnosis for patients suffering from breast cancer and several other disorders. It has the potential to evolve into an easily accessible screening modality and diagnostic technique for breast cancer through the use of portable neutron sources and portable gamma detectors. It can detect and identify malignant tissue in the breast and generate a two-dimensional image through a single non-invasive tomographic scan without the need for breast compression or biopsies. TO be able to detect concentrations of elements that are markers of cancer, significant improvements in sensitivity are required. Efforts are under way to achieve the micro-gram sensitivity while maintaining the lowest possible dose level delivered to the patient. Using high-flux sources and multiple detectors will increase detection efficiency and reduce scan time, which will both in turn reduce the time-dependent background and hence increase signal to noise ratio. Increased detection efficiency will also reduce patient dose. Our final goal is to implement a portable, low-dose breast cancer screening system to detect breast cancer without the need for breast compression or invasive biopsies.

## Acknowledgment

We thank all the members of the Triangle Universities Nuclear Laboratory for their help with data acquisition and the members of Duke Advanced Imaging Laboratories for their help with data analysis. We thank the Center for In-vivo Microscopy at Duke University for providing the fixed mouse specimen.

## REFERENCES


[1] C. E. Floyd, J. E. Bender, A. C. Sharma, A. J. Kapadia, J. Q. Xia, B. P. Harrawood, G. D. Tourassi, J. Y. Lo, A. S. Crowell, and C. R. Howell, "Introduction to neutron stimulated emission computed tomography," *Physics in Medicine and Biology*, vol. 51, pp. 3375-3390, 2006.

[2] C. E. Floyd, C. R. Howell, B. P. Harrawood, A. S. Crowell, A. J. Kapadia, R. Macri, J. Q. Xia, R. Pedroni, J. Bowsher, M. R. Kiser, G. D. Tourassi, W. Tornow, and R. Walter, "Neutron Stimulated Emission Computed Tomography of Stable Isotopes," presented at SPIE Medical Imaging, San Diego, CA, 2004.

[3] A. Garg, V. Singh, et al., "An elemental correlation study in cancerous and normal breast tissue with successive clinical stages by neutron activation analysis," *Biological Trace Element Research*, vol. 46, pp. 185-202, 1994.

[4] K. Geraki and M. Farquharson, "Concentrations of Fe, Cu and Zn in breast tissue: a synchrotron XRF study," *Phys. Med. Biol*, vol. 47, pp. 2327-2339, 2002.

[5] K. Geraki, M. J. Farquharson, and D. A. Bradley, "X-ray fluorescence and energy dispersive x-ray diffraction for the quantification of elemental concentrations in breast tissue," *Phys. Med. Biol*, vol. 49, pp. 99-110, 2004.

[6] H. Mussalo-Rauhamaa, S. Piepponen, J. Lehto, R. Kauppila, and O. Auvinen, "Cu, Zn, Se and Mg concentrations in breast fat of Finnish breast cancer patients and healthy controls," *Trace Elements in Medicine*, vol. 10, pp. 13-15, 1993.

[7] K.-H. Ng, D. Bradley, and L.-M. Looi, "Elevated trace element concentrations in malignant breast tissues," *British Journal of Radiology*, vol. 70, pp. 375-382, 1997.

[8] K.-H. Ng, S.-H. Ong, D. A. Bradley, and L.-M. Looi, "Discriminant analysis of normal and malignant breast tissue based upon INAA investigation of elemental concentration," *Appl. Radiat. Isot.*, vol. 48, pp. 105-109, 1997.

[9] S. Rizk and H. Sky-Peck, "Comparison between concentrations of trace elements in normal and neoplastic human breast tissue," *Cancer Research*, vol. 44, pp. 5390-5394, 1984.

[10] A. Schwartz and R. Fink, "Trace Elements in Normal and Malignant Human Breast Tissue," *Surgery*, vol. 76, pp. 325-329, 1974.

[11] M. Yaman, D. Atici, S. Bakirdere, and I. Akdeniz, "Comparison of trace metal concentrations in malign and benign human prostate," *J. Med. Chem.*, vol. 48, pp. 630-634, 2005.

[12] E. Andrasi, M. Suhajda, I. Saray, L. Bezur, L. Ernyei, and A. Reffy, "Concentration of elements in human brain: *glioblastoma multiforme*," *Sci Total Env*, vol. 139-140, pp. 399-402, 1993.

[13] J. D. Stedman and N. M. Spyrou, "Major and trace element concentration differences between right and left hemispheres of the 'normal' human brain," *Nutrition*, vol. 11, pp. 542-545, 1995.

[14] S. R. Hollan, "Transfusion-associated iron overload," *Curr Opin Hematol*, vol. 4, pp. 436-41, 1997.

[15] L. W. Powell and K. J. Isselbacher, "Hemochromatosis," in *Harrison's Principles of Internal Medicine*: McGraw-Hill.

[16] L. W. Powell, "Diagnosis of hemochromatosis," *Semin Gastrointest Dis*, vol. 13, pp. 80-8, 2002.

[17] L. W. Powell, D. K. George, S. M. McDonnell, and K. V. Kowdley, "Diagnosis of hemochromatosis," *Ann Intern Med*, vol. 129, pp. 925-31, 1998.

[18] C. E. Floyd, J. E. Bender, A. C. Sharma, A. J. Kapadia, J. Q. Xia, B. P. Harrawood, G. D. Tourassi, J. Y. Lo, and A. S. C. C. R. Howell, "Neutron Stimulated Emission Computed Tomography of a Multi-Element Phantom," *IEEE Trans Med Imag*, vol. submitted (2006), 2006.

# Non-Invasive Estimation of Potassium (39K) in Bovine Liver Using Neutron Stimulated Emission Computed Tomography (NSECT)

Anuj J. Kapadia, Amy C. Sharma, Georgia D. Tourassi, Janelle E. Bender, Alexander S. Crowell, Matthew R. Kiser, Calvin R. Howell, Carey E. Floyd Jr.

***Abstract*– Neutron stimulated emission computed tomography (NSECT) is being developed as a non-invasive technique to measure element concentration in in-vivo tissue at molecular levels. We have developed a system that performs this task using an incident neutron beam that scatters inelastically with an atomic nucleus causing it to emit a characteristic gamma photon. An energy-sensitive gamma detector is used to detect this energy and identify the target atom. Here we describe an experiment to determine the concentration of natural potassium (39K) in bovine liver without the need for a biopsy. A 5 MeV neutron beam was used to scan a known quantity of bovine liver to obtain a gamma spectrum showing element concentration in the liver. An aqueous KCl solution calibration sample was then scanned to establish a ratio of potassium concentration to gamma counts for the experimental setup. Counts from gamma peaks corresponding to excited states in 39K were summed and compared with counts from the known calibration sample, to give the concentration of 39K in the liver. A high purity germanium (HPGe) clover detector was used to measure the emitted gamma energy. The results were validated through neutron activation analysis (NAA) of the liver sample. The concentration of 39K reported by NSECT was found to be within 13% of the NAA result, clearly demonstrating the ability of NSECT for non-invasive quantification of element concentration in tissue.**

Manuscript received November 13, 2006. This work was supported by the NIH/NCI grant 1-R21-CA106873-01 and in part by Department of Defense (Breast Cancer Research Program) under award number W81XWH-06-1-0484.

A. J. Kapadia is with the Department of Biomedical Engineering and the Duke Advanced Imaging Laboratories (DAILabs) of the Department of Radiology, Duke University, Durham, NC 27710, USA (phone: 919-684-1470; fax: 919-684-1491; email: anuj.kapadia@duke.edu).

A.C. Sharma is with the Department of Biomedical Engineering and the DAILabs of the Department of Radiology, Duke University, Durham, NC 27710, USA (phone: 919-684-1471; fax: 919-684-1491; email: anc4@duke.edu).

G.D. Tourassi is with the DAILabs of the Department of Radiology, Duke University, Durham, NC 27710, USA (phone: 919-684-1447; fax: 919-684-1491; email: gt@deckard.duhs.duke.edu).

J. E. Bender is with the Department of Biomedical Engineering, Duke University, Durham, NC 27710, USA (email: janelle.bender@duke.edu).

A. S. Crowell is with the Department of Physics, Duke University and the Triangle Universities Nuclear Laboratory, Durham, NC 27708, USA (phone: 919-660-2639; fax: 919-660-2634; email: crowell@tunl.duke.edu).

M. R. Kiser is with the Department of Physics, Duke University and the Triangle Universities Nuclear Laboratory, Durham, NC 27708, USA (phone: 919-660-2639; fax: 919-660-2634; email: kiser@tunl.duke.edu).

C. R. Howell is with the Department of Physics, Duke University and the Triangle Universities Nuclear Laboratory, Durham, NC 27708, USA (phone: 919-660-2632; fax: 919-660-2634; email: howell@tunl.duke.edu).

C. E. Floyd Jr. is with the DAILabs of the Department of Radiology, Duke University Medical Center and the Department of Biomedical Engineering Duke University, Durham, NC 27710.

## I. Introduction

Neutron stimulated emission computed tomography (NSECT) is being developed as a non-invasive technique to measure element concentration in the human body. We have developed an NSECT system that identifies element concentrations in in-vivo biological tissue using a beam of fast neutrons [1-3]. The basic principle of NSECT is as follows: An incident neutron interacts with target atomic nuclei mainly through scattering. If the scattering is inelastic, the target nucleus gets excited to a higher energy state which is often unstable. The unstable nucleus then rapidly decays to its ground state, emitting the excess energy as a characteristic gamma photon. The energy of the emitted photon is equal to the difference between the two energy states, and is well known and unique to most elements and isotopes. Hence, it serves as a signature of the emitting atom and can be measured by an energy-sensitive gamma detector to identify the atom.

## II. Relevance and Motivation

Such non-invasive quantification of elements in the body shows great potential in diagnostic procedures associated with several disorders in humans. For example, hemochromatosis (liver iron overload associated with thalassemia and sickle cell anemia) and Wilson's disease (liver copper overload) are both characterized by increased element concentration in the liver [4]. Patients suffering from thalassemia and sickle cell anemia often require weekly blood transfusions. With each transfusion fresh iron enters the body while the old iron remains in it. Since the body does not have an effective method to get rid of excess iron, it starts accumulating in various organs, especially the liver. The preferred diagnostic procedure for liver overload disorders is liver biopsy [5, 6]. This is an unpleasant procedure that can have several potential complications in patients. Quantification results from biopsy suffer from a 20% margin of error in determining element concentration in tissue. There is a need for an alternative technique to measure hepatic element concentration non-invasively. Here we describe an experiment to non-invasively determine the concentration of an element in the liver.

## III. METHODS

This experiment was performed at the Triangle Universities Nuclear Laboratory (TUNL) accelerator lab, on Duke University's campus. The experimental setup has been described in detail elsewhere [1]. A brief description follows.

### A. Experimental Setup

A 5 MeV neutron beam was produced by a Van-de-Graaf accelerator through a $^{2}H(d,n)^{3}He$ reaction, by bombarding a deuterium gas target with a deuteron beam. This beam was then collimated to a cylindrical profile using copper collimators, and focused on the target bovine liver sample. A neutron flux monitor made up of a scintillator attached to a photo-multiplier tube counted the number of neutron particles reaching the target. The gamma photons emitted by the sample were counted by two high purity germanium (HPGe) clover detectors hooked up to a data acquisition system. Lead and borated paraffin wax shielding was used to shield the detector from scattered neutrons and gammas. The detectors were calibrated against known energy peaks from a radioactive $^{22}Na$ source. The neutron beam profile was measured to be cylindrical with a 6cm diameter corresponding to a beam area of $28.26cm^2$.

### B. Samples

Three samples were prepared and scanned using this experimental setup.

A calibration sample was prepared using an aqueous solution of 2.5g KCl and 2.5g NaCl in 40g $H_2O$, along with 5g of iron powder. It was determined that 1.22g of $^{39}K$ was present in the sample. This sample was scanned with the 6cm beam to determine a ratio of potassium concentration to gamma counts for this experimental setup.

The second sample comprised a bovine liver (392.5g) with an unknown concentration of $^{39}K$, placed inside a plastic container. The cylindrical plastic container measured 9cm in diameter and 7cm in height. Calculations showed that 177.7g of liver lay in the neutron beam path. This unknown sample was scanned using the same experimental setup to determine its elemental concentration.

A third sample comprising 40g $H_2O$ was scanned to provide a background spectrum to correct for sample-dependent background. Hydrogen atoms in water have the same mass as neutrons, and hence generate a lot of neutron scatter adding to sample-related noise. The normalized spectrum from this sample was used as the background which was subtracted from the other two spectrums.

### C. Background Correction

Each spectrum was background corrected using 3 techniques. First, time-of-flight correction was used to reduce time-uncorrelated background noise from random sources of activity in the beam room. Second, sample-related background was reduced by subtracting the normalized water spectrum from each of the other two spectrums. Finally, a polynomial curve fit was used to model and subtract the residual underlying background, which is an effect of the detector efficiency. A photon entering the detector may not deposit all its energy at once, but do so in stages instead, leading to an energy spread over the low energy channels in the detector.

Background corrected spectrums obtained from the calibration sample and bovine liver sample are shown in Fig. 1 and Fig. 2 respectively.

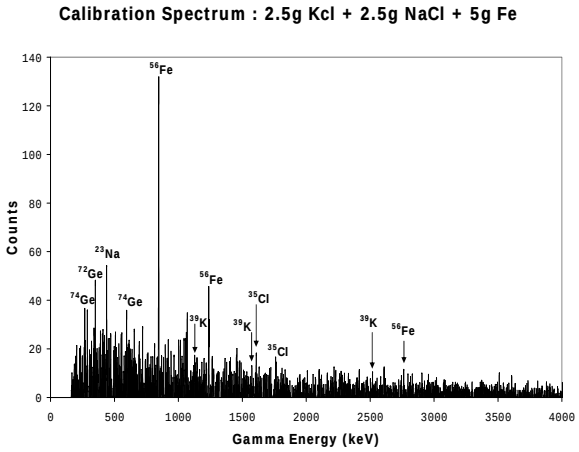


Fig.1. Gamma spectra showing peaks corresponding to excited states in various elements detected in the calibration sample. Gamma peaks are seen for $^{39}K$, $^{23}Na$, $^{35}Cl$, $^{37}Cl$, $^{56}Fe$, $^{70}Ge$, and $^{74}Ge$. These spectra are shown without neutron or gamma attenuation correction.

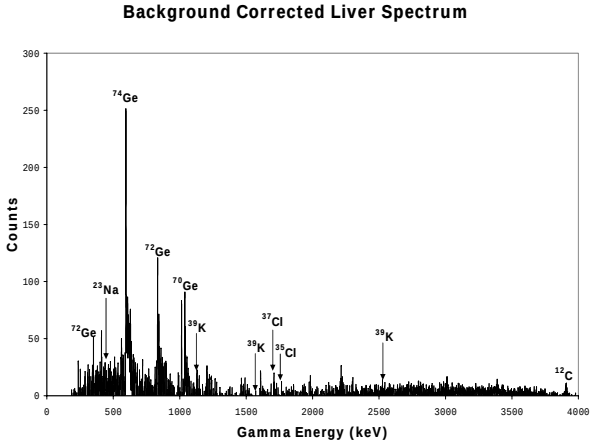


Fig.2. Gamma spectra showing peaks corresponding to excited states in various elements detected in the liver sample. Gamma peaks are identified for all the elements seen in the calibration sample, i.e. $^{39}K$, $^{23}Na$, $^{35}Cl$, $^{37}Cl$, $^{56}Fe$, $^{70}Ge$, and $^{74}Ge$. Peaks from $^{39}K$ are relatively isolated from neighboring peaks and can be used for quantification studies. These spectra are shown without neutron or gamma attenuation correction.

The calibration sample shows peaks from energy states in potassium ($^{39}K$), sodium ($^{23}Na$), chlorine ($^{35}Cl$, $^{37}Cl$), and iron ($^{56}Fe$). Peaks corresponding to natural states in germanium are seen from the HPGe detectors. Peaks from $^{39}K$ were seen to be relatively isolated from neighboring peaks and were hence used in this quantification study. The concentration of other

elements in the liver was too low to be detected accurately by this system.

To calculate the concentration of potassium in the liver, counts from energy peaks at 1130 keV and 1573 keV corresponding to excited states in $^{39}$K were summed and normalized against neutron flux monitor counts to get a normalized gamma count yield for both samples. Comparison of the gamma count yield from the unknown bovine liver to that of the calibration sample determined the concentration of $^{39}$K seen by the neutron beam in the bovine liver.

The bovine liver sample was sent for neutron activation analysis (NAA) to determine its elemental composition and provide an estimate of the potassium content to validate the results of this experiment. As expected, NAA showed that the other elements seen in the calibration sample, i.e. $^{39}$K, $^{23}$Na, $^{35}$Cl, $^{37}$Cl and $^{56}$Fe were present in extremely low concentrations in the liver sample. NAA scanning was performed on a wet sample.

## IV. Results and Conclusion

Using the ratio of potassium concentration to gamma counts determined for the calibration sample, the liver potassium concentration was estimated to be 3.37 mg/g wet liver. The NAA results estimated the potassium concentration to be 3.0 mg/g wet liver. The result obtained through NSECT was within 13% of that reported by NAA, an accepted standard element analysis technique. This experiment clearly demonstrates NSECT's ability to non-invasively estimate element concentration in biological tissue. Efforts are being made to improve the sensitivity of the system and detect elements present in low concentrations. Some of the errors in this system can be attributed to a low detection efficiency, high noise background, neutron and gamma attenuation by the samples, and loss of statistical accuracy due to overlapping peaks. Detection efficiency can be improved by using multiple detectors and high flux neutron sources, both of which will also reduce overall scan time. While patient dose for this experiment was calculated to be approximately 15 mSv, increasing detection efficiency will help reduce patient dose even further. Future work includes implementing attenuation correction techniques for both neutron and gamma attenuation in the sample and implementing mathematical peak-fitting algorithms to separate overlapping energy peaks.

## Acknowledgment

We thank all the members of the Triangle Universities Nuclear Laboratory for their help with data acquisition and the members of Duke Advanced Imaging Laboratories for their help with data analysis.

## References

[1] C. E. Floyd, J. E. Bender, A. C. Sharma, A. J. Kapadia, J. Q. Xia, B. P. Harrawood, G. D. Tourassi, J. Y. Lo, A. S. Crowell, and C. R. Howell, "Introduction to neutron stimulated emission computed tomography," *Physics in Medicine and Biology*, vol. 51, pp. 3375-3390, 2006.

[2] C. E. Floyd, J. E. Bender, A. C. Sharma, A. J. Kapadia, J. Q. Xia, B. P. Harrawood, G. D. Tourassi, J. Y. Lo, and A. S. C. C. R. Howell, "Neutron Stimulated Emission Computed Tomography of a Multi-Element Phantom," *IEEE Trans Med Imag*, vol. submitted (2006), 2006.

[3] C. E. Floyd, C. R. Howell, B. P. Harrawood, A. S. Crowell, A. J. Kapadia, R. Macri, J. Q. Xia, R. Pedroni, J. Bowsher, M. R. Kiser, G. D. Tourassi, W. Tornow, and R. Walter, "Neutron Stimulated Emission Computed Tomography of Stable Isotopes," presented at SPIE Medical Imaging, San Diego, CA, 2004.

[4] L. W. Powell and K. J. Isselbacher, "Hemochromatosis," in *Harrison's Principles of Internal Medicine*: McGraw-Hill.

[5] L. W. Powell, "Diagnosis of hemochromatosis," *Semin Gastrointest Dis*, vol. 13, pp. 80-8, 2002.

[6] L. W. Powell, D. K. George, S. M. McDonnell, and K. V. Kowdley, "Diagnosis of hemochromatosis," *Ann Intern Med*, vol. 129, pp. 925-31, 1998.

# Neutron Spectroscopy of Mouse Using Neutron Stimulated Emission Computed Tomography (NSECT)

Anuj J. Kapadia, Amy C. Sharma, Georgia D. Tourassi, Janelle E. Bender, Alexander S. Crowell, Matthew R. Kiser, Calvin R. Howell, Carey E. Floyd Jr.

***Abstract*– Neutron spectroscopy is evolving as a non-invasive technique to measure element concentration in biological tissue. We have developed a neutron stimulated emission computed tomography (NSECT) system that maps the elemental composition of a body through a non-invasive scan. A neutron beam incident on a sample energizes the sample's atomic nuclei through inelastic scatter interactions. These energized nuclei then spontaneously return to their ground energy states emitting the extra energy as a characteristic gamma photon. An energy-sensitive gamma detector is used to detect this energy and hence identify the emitting atom. Such a technique has several applications in both humans and small animals. Here we demonstrate NSECT's feasibility in scanning small animals, and show results from a spectroscopic examination of a fixed mouse specimen. The mouse was flushed with saline and fixed using a gadolinium/formalin solution. Scanning was performed using a 5 MeV monochromatic neutron beam. Background was corrected using time-of-flight correction to reduce time-uncorrelated noise and polynomial curve-fit subtraction to remove the residual underlying background. The emitted gammas were measured using a high purity germanium (HPGe) clover detector. The resulting spectrum shows various peaks corresponding to elements expected in this specimen such as C, Ca and Gd, several other potential matches such as K and Zn, as well as some system related elements such as Fe, Al and Ge from the detector. This experiment demonstrates the ability of NSECT to obtain element information from an intact small animal specimen through a single non-invasive scan.**

## I. Introduction

NEUTRON spectroscopy is evolving as a non-invasive technique to determine element concentrations in biological tissue. We have developed a neutron stimulated emission computed tomography system (NSECT) to identify element concentrations of in-vivo tissue using inelastic scattering of fast neutrons by target nuclei [1, 2]. A neutron incident on a target atom often scatters inelastically with the target atomic nucleus, exciting it to a higher unstable energy state. The unstable nucleus then rapidly decays to its ground state, emitting the excess energy as a characteristic gamma photon. The energy of the gamma photon is equal to the energy difference between the ground state and the excited state. These energy states are well-known and quantified for most known elements and isotopes and their energy difference therefore serves as a signature of the emitting atom. Thus, measuring the energy of the emitted gamma photon identifies the emitting atom and its concentration in the tissue sample.

## II. Relevance

Such a technique for spectroscopic evaluation of elements in tissue has several applications in both humans and small animals.

First, there are several disorders in humans which are associated with an increase in element concentration within the affected organ. For example, hemochromatosis which is an iron overload disorder associated with thalassemia and sickle cell anemia, is characterized by an increase in iron concentration in the liver [3, 4]. Wilson's disease shows an increase in the concentration of copper in the liver. These disorders both require element quantification for diagnosis, which is currently done through a liver biopsy [5, 6]. Biopsy is an unpleasant procedure which also has several potential complications associated with it. Despite being the current preferred diagnostic technique for these disorders, it has limitations in being used widely in patients suffering from these disorders due to its invasive nature. NSECT has the ability to diagnose iron and copper concentration changes in

Manuscript received November 13, 2006. This work was supported by the NIH/NCI grant 1-R21-CA106873-01 and in part by Department of Defense (Breast Cancer Research Program) under award number W81XWH-06-1-0484.

A. J. Kapadia is with the Department of Biomedical Engineering and the Duke Advanced Imaging Laboratories (DAILabs) of the Department of Radiology, Duke University, Durham, NC 27710, USA (phone: 919-684-1470; fax: 919-684-1491; email: anuj.kapadia@duke.edu).

A.C. Sharma is with the Department of Biomedical Engineering and the DAILabs of the Department of Radiology, Duke University, Durham, NC 27710, USA (phone: 919-684-1471; fax: 919-684-1491; email: anc4@duke.edu).

G.D. Tourassi is with the DAILabs of the Department of Radiology, Duke University, Durham, NC 27710, USA (phone: 919-684-1447; fax: 919-684-1491; email: gt@deckard.duhs.duke.edu).

J. E. Bender is with the Department of Biomedical Engineering, Duke University, Durham, NC 27710, USA (email: janelle.bender@duke.edu).

A. S. Crowell is with the Department of Physics, Duke University and the Triangle Universities Nuclear Laboratory, Durham, NC 27708, USA (phone: 919-660-2639; fax: 919-660-2634; email: crowell@tunl.duke.edu).

M. R. Kiser is with the Department of Physics, Duke University and the Triangle Universities Nuclear Laboratory, Durham, NC 27708, USA (phone: 919-660-2639; fax: 919-660-2634; email: kiser@tunl.duke.edu).

C. R. Howell is with the Department of Physics, Duke University and the Triangle Universities Nuclear Laboratory, Durham, NC 27708, USA (phone: 919-660-2632; fax: 919-660-2634; email: howell@tunl.duke.edu).

C. E. Floyd Jr. is with the DAILabs of the Department of Radiology, Duke University Medical Center and the Department of Biomedical Engineering Duke University, Durham, NC 27710.

the liver through a non-invasive scan, which could significantly reduce the need for liver biopsies.

Second, various experiments conducted on trace elements in humans and animals have shown that changes in concentration of trace elements are often associated with cancer in very early stages of development [7-10]. These concentration changes are seen in elements such as aluminum, iron, zinc, copper, rubidium, gold, silver and antimony, and have been observed as a pre-cursor to malignancy. Identifying the concentrations of these elements could potentially enable diagnosis of cancer very early, much before the tumor grows large enough to be detected through other conventional imaging techniques such as CT or mammography.

Finally, in small animals, NSECT's ability to detect element concentrations can be used to follow metabolic migration of nutrients or in normal and genetically modified mice or drug delivery in normal and modified tissue all without the need to tag molecules of interest with radioactive isotope tracers. NSECT has the ability to detect stable isotopes which occur naturally in these molecules which eliminates the need for radioactive tracers. It can also be used to measure iron and calcium levels in the cardiac wall.

## III. Motivation

The first step towards imaging small animals through NSECT is to demonstrate its feasibility in small animal imaging. Small animals have lower concentrations of elements such as carbon and calcium, which are otherwise found in greater quantities in humans. Low concentrations pose a challenge in detection due to the several reasons. The signal from low concentrations is low, which then requires a longer scan time to obtain adequate statistical accuracy. The increased scan time in turn increases the background noise and reduces the signal to noise ratio further. To demonstrate feasibility of small animal imaging, we have scanned and obtained a gamma spectrum from an intact biological specimen of a fixed mouse. Here we show results from the spectroscopic examination of the mouse and comment about NSECT's feasibility in imaging small animals.

## IV. Methods

This experiment was performed at the Triangle Universities Nuclear Laboratory (TUNL) accelerator lab, on Duke University's campus. Since the experimental setup has been described in detail elsewhere [1], only a brief description is included here.

A 5 MeV monochromatic neutron beam was produced through a $^{2}H(d,n)^{3}He$ reaction by using a Van-de-Graaf accelerator to bombard a deuterium gas target with accelerated deuterons. The emerging neutrons were then collimated using copper collimators, and focused on the target mouse specimen. A neutron flux monitor made up of a scintillator attached to a photo-multiplier tube counted the number of neutrons incident on the target. Two high purity germanium (HPGe) clover detectors were used to count the gamma photons emitted by the sample. Lead and paraffin wax blocks were used to shield the detector from unwanted neutrons and gammas. The detectors were calibrated against known energy peaks from a radioactive $^{22}Na$ source. The neutron beam profile was measured to be cylindrical with a 6cm diameter, corresponding to a beam area of $28.26cm^2$.

The mouse specimen was prepared for scanning as follows. A freshly sacrificed mouse was flushed with saline and then fixed for one week using a 1:10 gadolinium/formalin solution. After flushing the fixed mouse with saline once again, it was enclosed in a glass tube along with diluted formalin solution and sealed. This enclosed specimen was scanned for 95 minutes with the 5 MeV monochromatic neutron beam.

A second sample of 40g $H_2O$ was then scanned to provide a background spectrum to correct for sample-dependent background. Hydrogen atoms in water (which forms a large part of tissue) have the same mass as neutrons, and hence generate a lot of neutron scatter which adds to sample-related noise. Neutrons that scatter elastically off of the hydrogen atoms still carry a large part of their original energy, and can interact and generate inelastic scatter gamma photons from other materials present in the room, such as the detectors and sample mounting hardware. The spectrum from this water sample was normalized to incident neutron flux and used as background which was subtracted from the mouse spectrum.

Each spectrum was background corrected using three correction techniques. First, time-of-flight correction was used to reduce time-uncorrelated background noise from random sources of activity in the beam room. Second, sample-related scatter background was reduced by subtracting the normalized water spectrum from the mouse spectrum. Finally, a polynomial curve fit was used to model and subtract the residual underlying background, which is an effect of the detector efficiency. A photon entering the detector may not deposit all its energy at once, but instead do so in stages, leading to a greater energy spread over the lower energy channels of the detector.

As this was an experiment to demonstrate feasibility, no quantitative analysis was performed on the detected elements. Quantitative analysis would require obtaining calibration spectra from known quantities of element samples under conditions similar to those of the unknown specimen (fixed mouse in this case). Quantitative analysis has been performed in other experiments and described elsewhere [11].

## V. Results

The background corrected spectrum from the fixed mouse specimen is shown in Fig 1. Gamma peaks were observed for various elements expected from the mouse specimen as well as from materials expected in the system. Energy peaks were identified for $^{12}C$ from tissue, $^{40}Ca$ from bone, and elements $^{39}K$, $^{27}Al$, $^{37}Cl$, $^{56}Fe$, $^{68}Zn$ and $^{25}Mg$ which could potentially be present in the specimen. The elements $^{27}Al$ and $^{56}Fe$ could also be system dependent as many components used to mount the detectors and other hardware were made of aluminum and iron. Energy peaks were identified for $^{158}Gd$ and $^{160}Gd$ from the 1:10 gadolinium/formalin fixing solution in the sample,

along with energy peaks from several naturally occurring states in germanium from the HPGe detectors.

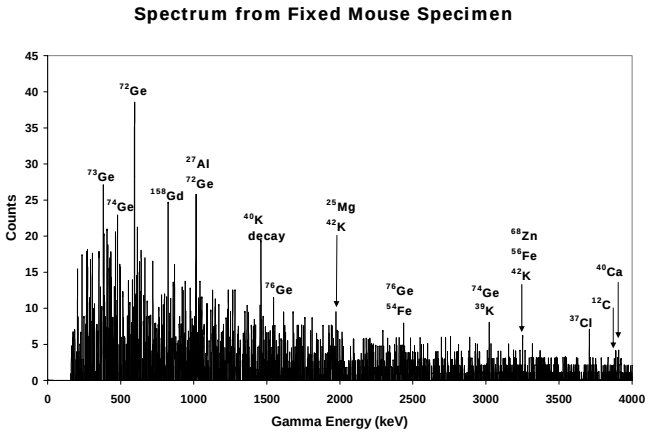


Fig.1. Gamma spectrum from a formalin fixed mouse specimen showing peaks corresponding to excited states in various elements. Gamma peaks are seen for $^{12}$C (escape peaks), $^{40}$Ca, $^{39}$K, $^{27}$Al, $^{37}$Cl, $^{56}$Fe, $^{68}$Zn and $^{25}$Mg. Gamma peaks are also seen for $^{72}$Ge and $^{74}$Ge from the germanium detector, and $^{158}$Gd and $^{160}$Gd from the fixing solution. Peaks with multiple potential element matches are labeled accordingly. These spectra are shown without neutron or gamma attenuation correction.

## VI. Conclusion

This experiment demonstrates the ability of NSECT to obtain an elemental map of an intact small-animal specimen through a non-invasive scan. To cross-check the presence of potential elements, the mouse specimen will be sent for Neutron Activation Analysis (NAA) which will return quantitative analyses of elements present in this individual specimen. While a few of the dominant element peaks are system related, peaks corresponding to elements known to be present in the mouse specimen are also seen.

Sources of error in the system currently include high scan time, low detection efficiency and high background noise, all of which reduce the sensitivity of the system. Efforts are being made to improve the overall sensitivity of the system to be able to detect low concentration elements in the specimen. Scan time can be reduced greatly by using commercial neutron sources with high neutron flux, and using multiple detectors to acquire data. These two factors will greatly reduce the overall scan time, which in turn will reduce time-related background noise and improve the signal to noise ratio. Shorter scans with multiple detectors will also improve detection efficiency and reduce patient dose.

## Acknowledgment

We thank all the members of the Triangle Universities Nuclear Laboratory for their help with data acquisition and the members of Duke Advanced Imaging Laboratories for their help with data analysis. We thank the Center for In-vivo Microscopy at Duke University for providing the fixed mouse specimen.

## References

[1] C. E. Floyd, J. E. Bender, A. C. Sharma, A. J. Kapadia, J. Q. Xia, B. P. Harrawood, G. D. Tourassi, J. Y. Lo, A. S. Crowell, and C. R. Howell, "Introduction to neutron stimulated emission computed tomography," *Physics in Medicine and Biology*, vol. 51, pp. 3375-3390, 2006.

[2] C. E. Floyd, C. R. Howell, B. P. Harrawood, A. S. Crowell, A. J. Kapadia, R. Macri, J. Q. Xia, R. Pedroni, J. Bowsher, M. R. Kiser, G. D. Tourassi, W. Tornow, and R. Walter, "Neutron Stimulated Emission Computed Tomography of Stable Isotopes," presented at SPIE Medical Imaging, San Diego, CA, 2004.

[3] N. C. Andrews, "Disorders of iron metabolism," *N Engl J Med*, vol. 341, pp. 1986-95, 1999.

[4] L. W. Powell and K. J. Isselbacher, "Hemochromatosis," in *Harrison's Principles of Internal Medicine*: McGraw-Hill.

[5] L. W. Powell, "Diagnosis of hemochromatosis," *Semin Gastrointest Dis*, vol. 13, pp. 80-8, 2002.

[6] L. W. Powell, D. K. George, S. M. McDonnell, and K. V. Kowdley, "Diagnosis of hemochromatosis," *Ann Intern Med*, vol. 129, pp. 925-31, 1998.

[7] A. Danielsen and E. Steinnes, "A study of some selected trace elements in normal and cancerous tissue by neutron activation analysis," *J Nuclear Medicine*, vol. 11, pp. 260-264, 1970.

[8] A. Garg, V. Singh, et al., "An elemental correlation study in cancerous and normal breast tissue with successive clinical stages by neutron activation analysis," *Biological Trace Element Research*, vol. 46, pp. 185-202, 1994.

[9] H. Mussalo-Rauhamaa, S. Piepponen, J. Lehto, R. Kauppila, and O. Auvinen, "Cu, Zn, Se and Mg concentrations in breast fat of Finnish breast cancer patients and healthy controls," *Trace Elements in Medicine*, vol. 10, pp. 13-15, 1993.

[10] S. Rizk and H. Sky-Peck, "Comparison between concentrations of trace elements in normal and neoplastic human breast tissue," *Cancer Research*, vol. 44, pp. 5390-5394, 1984.

[11] A. J. Kapadia, C. E. Floyd, J. E. Bender, C. R. Howell, A. S. Crowell, and M. R. Kiser, "Non-invasive quantification of iron 56-Fe in beef liver using neutron stimulated emission computed tomography," presented at IEEE Nuclear Science Symposium Conference, Puerto Rico, 2005.

# Neutron Stimulated Emission Computed Tomography for Diagnosis of Breast Cancer

Anuj J. Kapadia, Amy C. Sharma, Georgia D. Tourassi, Janelle E. Bender, Calvin R. Howell, Alexander S. Crowell, Matthew R. Kiser, Brian P. Harrawood, Carey E. Floyd Jr.

***Abstract*— Neutron stimulated emission computed tomography (NSECT) is being developed as a non-invasive spectroscopic imaging technique to determine element concentrations in the human body. We have implemented an NSECT system that uses a beam of high-energy neutrons to identify element concentrations in tissue and create 2-dimensional maps of elemental distribution through a single non-invasive tomographic scan. NSECT uses a beam of fast neutrons that scatter inelastically with atomic nuclei in tissue, causing them to emit characteristic gamma photons that are detected and identified using an energy-sensitive gamma detector. By measuring the energy and number of emitted gamma photons, the system can determine the elemental composition of the target tissue. Such determination is useful in detecting several disorders in the human body that are characterized by changes in element concentration, one of which is breast cancer. NSECT has the advantage of being able to detect breast cancer at very early stages compared to anatomic screening techniques as it detects changes in trace element concentrations in the breast which are usually seen before tumors and micro-calcifications appear. In this paper we describe our experimental implementation of NSECT for the diagnosis of breast cancer and investigate its feasibility in detecting elements in breast tissue at concentrations relevant to clinical scenarios. Results are shown from preliminary scans of breast tissue samples and a mixed sample used for determining the detection threshold of NSECT. A spectrum from a small-animal specimen is also included to demonstrate detection ability from in-vivo tissue. Our preliminary results indicate that NSECT has the ability to detect elements in breast tissue. Currently, the threshold value determined is much higher than the microgram sensitivity required for cancer detection. However, with some improvement in sensitivity, NSECT has the potential to develop into a breast cancer diagnosis technique. Efforts are under way to improve detection sensitivity while maintaining the lowest possible dose delivered to the patient. Patient dose levels from NSECT are comparable to those of screening mammography. Our final goal is to implement a portable, low-dose tomographic screening system for breast cancer, which does not require breast compression or invasive biopsies.**

***Index Terms*—Breast Cancer Detection, Gamma-ray spectroscopy, Neutron, Tomography.**

Manuscript received January 5, 2007. This work was supported by the NIH/NCI grant 1-R21-CA106873-01 and in part by Department of Defense (Breast Cancer Research Program) under award number W81XWH-06-1-0484.

A. J. Kapadia is with the Department of Biomedical Engineering and the Duke Advanced Imaging Laboratories (DAILabs) of the Department of Radiology, Duke University (Mailing Address: 2424 Erwin Road, Suite 302, Durham, NC 27705, USA; phone: 919-684-1470; fax: 919-684-1491; email: anuj.kapadia@duke.edu).

A.C. Sharma is with the Department of Biomedical Engineering and the DAILabs of the Department of Radiology, Duke University, Durham, NC 27710, USA (email: anc4@duke.edu).

G.D. Tourassi is with the DAILabs of the Department of Radiology, Duke University, Durham, NC 27710, USA (email: gt@deckard.duhs.duke.edu).

J. E. Bender is with the Department of Biomedical Engineering, Duke University, Durham, NC 27710, USA (email: janelle.bender@duke.edu).

C. R. Howell is with the Department of Physics, Duke University and the Triangle Universities Nuclear Laboratory, Durham, NC 27708, USA (email: howell@tunl.duke.edu).

A. S. Crowell is with the Department of Physics, Duke University and the Triangle Universities Nuclear Laboratory, Durham, NC 27708, USA (email: crowell@tunl.duke.edu).

M. R. Kiser is with the Department of Physics, Duke University and the Triangle Universities Nuclear Laboratory, Durham, NC 27708, USA email: kiser@tunl.duke.edu).

B.P.Harrawood is with the DAILabs of the Department of Radiology, Duke University, Durham, NC 27710, USA (email: brian.harrawood@duke.edu).

C. E. Floyd Jr. is with the DAILabs of the Department of Radiology, Duke University Medical Center and the Department of Biomedical Engineering Duke University, Durham, NC 27710.

## I. Introduction

NEUTRON techniques are rapidly evolving as methods of measuring trace element concentrations in the human body [1-6] as well as in animal tissue [7, 8]. We have successfully implemented a tomographic non-invasive in-vivo imaging technique called Neutron Stimulated Emission Computed Tomography (NSECT) to obtain two-dimensional tomographic information about element concentration within a target tissue sample [9-17]. NSECT uses spectral information obtained from inelastic scattering reactions between neutrons and atomic nuclei in the target sample to identify the target atoms and determine their concentration in-vivo.

Such a technique has several potential applications in both humans and small animals. Several studies have indicated that changes in trace element concentrations in human tissue may be a precursor to malignancy [1, 5, 6, 18-20]. These concentration changes have the ability to differentiate between malignant and benign tissue, and their quantification could enable *in-vivo* cancer diagnosis at very early stages. Element concentration changes have also been observed for iron in diseases such as sickle cell anemia, thalassemia major, hemosiderosis and hemochromatosis [21-27] and in copper for Wilson's disease [28]. NSECT has the potential to image element concentrations in tomographic regions of interest

within affected organs, which can help diagnose and follow the progress of these disorders.

The underlying NSECT principle is the following. NSECT relies on inelastic scatter reactions that occur when atomic nuclei are bombarded with fast neutrons. When an incident neutron scatters inelastically with a target atomic nucleus, the nucleus gets excited to one of its quantized higher-energy states which is often unstable. This excited nucleus then rapidly decays to a lower state, emitting a gamma ray photon whose energy is equal to the difference between the energies of the two states. These non-overlapping energy states are well established and somewhat unique to each element and isotope. Detection and analysis of the emitted gamma spectrum can thus be used to identify the emitting target atom.

Emitted gamma photons are captured using an energy-sensitive gamma detector. Tomography is currently performed by acquiring a complete set of projections of line integrals using the translate-rotate configuration as in first generation CT scanners, i.e. the beam is translated horizontally through the entire sample length, then the sample is rotated through some fixed angle and the process is repeated. This tomographic scanning technique yields a two-dimensional map of element concentration and distribution within the sample. The translate-rotate geometry is appropriate for initial proof of concept studies using phantoms, specimens or small animals. Once feasibility is demonstrated, other geometries can be used in future clinical systems. Images are reconstructed using the Maximum Likelihood Expectation Maximization algorithm, an iterative technique to optimize an image reconstructed from a finite set of its projections [29-31].

NSECT has tremendous potential in diagnosis of several disorders in the human body that are characterized by changes in element concentration in the affected organ or tissue. Its advantage lies in its two-fold ability to (i) non-invasively determine the elemental composition within a tomographic region of interest in tissue, and (ii) image stable isotopes already present inside the body, eliminating the need to inject radioactive tracers. One of the disorders of interest, which is characterized by changes in element concentration in the affected tissue, is breast cancer.

Breast cancer is the leading type of non-skin cancer to affect women and the second most common cause of cancer deaths in women [32]. In the United States alone, breast cancer is expected to account for 31% of all new cancer cases among women [33]. The American Cancer Society estimated that 212,920 cases of invasive breast cancer will be detected in 2006, and 41,430 of these will result in death [33]. Early detection has proved to be the most effective technique to increase survival rates for this disease.

Screening x-ray mammography is at present the only FDA approved screening tool for breast cancer screening. While it has proved to be effective, screening mammography has several limitations in detecting masses and spiculations in mammograms. First, it requires that the mammograms have good contrast, which is often difficult to achieve in women with dense breasts. Second, it uses an anatomic approach in trying to identify abnormalities in mammograms, making it essential that the abnormality be developed enough to show masses and calcifications clearly; a development that usually comes at advanced stages of tumor growth. Finally, mammography has limitations in classifying detected abnormalities as benign or malignant. Over 70% of detected abnormalities sent for biopsy turn out to be benign [34]. Several artificial intelligence tools, developed to classify detected lesions as benign or malignant have been investigated, but none have been FDA approved yet. These tools, such as computer aided diagnosis, make their decisions based on morphological features such as shape, size and texture. While they are fairly effective in classifying a detected lesion as benign or malignant, their dependence on analyzing an already visible lesion reduces their decision-making ability for lesions in very early stages of development. NSECT's sensitivity to metabolic changes seen in malignant tumors in very early developmental stages has the potential to overcome the disadvantages of screening mammography.

Several studies have demonstrated that breast cancer is associated with changes in trace element concentration in the malignant tissue at very early stages. These changes have been observed in concentration of elements such as Al, Br, Ca, Cl, Co, Cs, Cu, Fe, K, Mn, Na, Rb, Sb, Se and Zn, and often occur much earlier than morphologic changes such as tumors and calcifications begin to appear [1, 6, 18-20, 35]. Quantifying these element concentrations could potentially enable diagnosis of breast cancer much before the tumor grows large enough to be detected by existing imaging techniques. Generally, NSECT's role in diagnosing breast cancer is to (i) spectroscopically quantify the concentration of elements of interest in the tissue to diagnose the disorder, and (ii) generate three dimensional tomographic image of the element concentration in the organ to isolate the region affected by the disorder. As most of these trace elements occur in the body in microgram quantities, a primary objective of this study is to determine whether NSECT has the required sensitivity to detect micro-gram concentration changes in-vivo.

In this paper we describe our experimental implementation of NSECT for the diagnosis of breast cancer. While our eventual goal is to implement the NSECT system in a configuration that can be employed in a clinical environment for non-invasive detection and monitoring of diseases, here we investigate NSECT's feasibility in detecting element concentration changes in human tissue at concentrations that are relevant to clinical scenarios. The manuscript is organized as follows. Section II describes the lab resources and equipments used. Section III shows spectral results from preliminary scans in breast biopsy samples. Section IV discusses the study findings, possible limitations and improvements, and conclusion. A brief discussion regarding patient dose is also included.

## II. MATERIALS AND METHODS

### *A. Facilities and Equipment*

NSECT experiments have been performed at the Triangle Universities Nuclear Laboratory (TUNL) accelerator lab

located on Duke University's campus. TUNL is a medium energy nuclear structure laboratory with a variety of charged particle sources, and a 10 megavolt Tandem Van De Graff accelerator capable of producing 20MeV proton or deuteron beams and a host of other light projectile beams. Its "shielded neutron source" produces a large pulsed mono-energetic neutron beam behind a meter thick shielding wall with variable size collimator inserts, to allow a neutron beam to be produced with diameter ranging from 1mm to 60mm. The shielding allows sensitive detectors to be used without extensive additional shielding to enhance the signal to noise (SNR) of the measurements. The key NSECT components are described below.

*1) Neutron Source*

Neutrons are produced through the $^{2}H(d,n)^{3}He$ reaction by directing an accelerated and pulsed beam of negatively charged deuterons onto a deuterium gas target. The deuterons are accelerated by a 10 megavolt tandem Van-de-Graaf accelerator capable of accelerating particles through 20 MeV. Negatively charged deuterons are focused onto the positively charged tandem Van-de-Graaf accelerator which accelerates them through 10 MeV. As they reach the centre of the tandem, they pass through a thin positively charged carbon foil that strips them of two electrons, creating a net positive charge. The now positively charged deuterons are further accelerated through 10 MeV as they leave the tandem. Thus, depending on the charge setting on the tandem, the deuteron beam can be accelerated anywhere between 3 and 20 MeV. Beam steering is performed on the charged deuteron beam using two sets of magnetic steering coils, one located before and the other after the tandem.

The charged deuteron beam is then directed onto a pressurized deuterium gas cell located behind a meter-thick shielding wall composed of concrete, steel, lead, and paraffin loaded with boron and lithium. Neutrons created through the ddn reaction ($D + {}^{2}H \rightarrow {}^{3}He + {}^{1}n$ ; Q= 3.26 MeV) are highly forward peaked and have monochromatic beam energy adjustable between 5 and 23.2 MeV.

The beam then passes through the shielding wall through a collimated channel made of copper. Copper is chosen because it adequately attenuates neutrons, is fairly simple to machine and is reasonably low cost. The collimator has swappable inserts that can be used in combinations to obtain beams ranging from 1 sq. mm to 60 sq. mm in area.

The beam is pulsed to provide 1 nanosecond wide bunches at the target to allow measurement of neutron and gamma time of flight, enabling time-of-flight background correction.

*2) Neutron Flux Monitor*

After exiting the collimator channel, the beam is incident on a thin neutron flux monitor placed between the collimator exit and the sample. The flux monitor is made up of a thin plastic neutron-scintillator attached to a photomultiplier tube, which is calibrated to report the neutron flux incident on the target. The 1.6 mm thickness of the scintillator ensures that neutron beam is not significantly attenuated as it passes through. The high voltage photomultiplier tube is calibrated to a ratio that incorporates the efficiency of the plastic scintillator. This calibration is done with respect to an argon detector (5” diameter x 0.74” thick) containing liquid scintillator (BC519), which is placed at zero degrees with respect to the neutron beam. The detection efficiency and position of this detector are known fairly accurately, and hence this detector can be used to measure neutron flux accurately. However, its size and attenuation of the neutron beam prohibits it from being placed between the sample and the exit of the collimator. Knowledge of the incident neutron flux is required for normalizing the acquired gamma data, to compensate for fluctuations in the deuteron source that lead to changes in incident neutron flux.

The zero degree liquid-scintillator argon detector is also used to obtain a neutron transmission image of the sample, which is required for attenuation correction.

*3) Sample Manipulator*

A computer-controlled sample holder allows precise horizontal, vertical and rotational positioning of small samples remotely. This holder allows tomographic acquisition by translating and rotating the sample with respect to the neutron beam. As mentioned earlier, tomography is performed through the translate-rotate geometry to obtain a complete set of line integrals through a slice of the sample. The projection-slice theorem states that an object’s density can be reconstructed from a complete set of projections of line integrals taken through the object. For neutron stimulated emission computed tomography, these projections are defined by the angular and spatial sampling intervals between successive positions of the sample as positioned by the sample manipulator. For our experiments, we used two Velmex Linear Bislides MN10-0050-M02-21 coupled together to provide 5 inches of motion in the horizontal and vertical directions, and a Velmex Rotary Table B4872TS to provide angular rotation. These were controlled using Velmex VXM2 Stepper Motor Controllers connected through serial cables to a PC running Velmex COSMOS controller software.

*4) Gamma Detectors*

Two high-purity germanium detectors were used to detect gamma photons emitted from the sample. These detectors are the 2-Fold Segmented Clover Detectors (CLOVER 4x50x80 SEG2) manufactured by Canberra Eurysis S.A. Each detector consists of four co-axial n-type germanium crystals mounted together in the shape of a 4-leaf clover. Each germanium crystal is 50mm in diameter and 80mm in length, with minimum relative efficiency of 22% and full width at half maximum less than or equal to 2.25 keV for 1.33 MeV gamma rays of $^{60}Co$. Both detectors were calibrated against known energy peaks from a $^{22}Na$ source and positioned at 135 degrees from the incident neutron beam at a distance of 20 cm from the sample. A majority of the states of interest decay by an electric quadrupole transition whose distribution has a maximum intensity at about 45 and 135 degrees. Using the 135 degree orientation helps prevent the gamma detector from being illuminated by either the direct neutron beam or by neutrons that elastically scatter from the target. An enclosure of lead bricks and lithium-loaded paraffin wax is used to shield the active area of the detector from the exit area of the collimator.

A schematic drawing of this configuration is shown in figure 1.

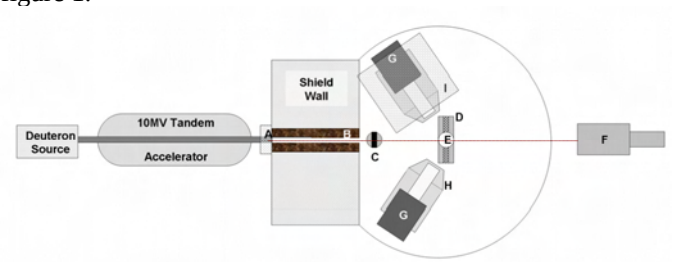


Fig 1. Schematic drawing of the experimental setup used in NSECT data acquisition. Components are labeled as follows:
A – Deuterium Gas Cell; B – Copper Collimator; C – Neutron Flux Monitor; D – Sample Manipulator; E – Sample; F – Zero-degree LS Argon Detector; G – HPGe detector; H – Anti-coincidence Shield; I – Detector Shielding Enclosure.

*5) Shielding*

The gamma detector is shielded from the neutron source by a meter-thick wall composed of concrete, steel, lead, borated plastic and lithium-loaded paraffin. In addition to this wall, an enclosure of lead bricks and lithium-loaded paraffin is built around each detector to shield the active area of the detector from neutrons scattering off of the exit edge of the collimator and the gammas created subsequently. Considerable effort is being devoted to optimizing shielding to reduce backgrounds in the gamma detectors.

*6) Computers and Acquisition Software*

Data was acquired on Pentium 4 PC's running Red Hat's Linux operating system using SpecTcl, a nuclear event data analysis tool developed at the National Superconducting Cyclotron Laboratory at Michigan State University. SpecTcl allows acquisition and storage of raw data using an object oriented C++ framework, and allows online and offline data visualization through the Xamine display program. Complete as well as partial sets of raw data can be retrieved at any time, including during acquisition, and analyzed using any desired set of parameters. The Xamine display program allows simultaneous display of multiple spectra including spectrum overlay. Data is transported between computers through local area network hardware and Ethernet with standard network protocols (TCP/IP).

*7) Amplifiers*

Canberra 2026 spectroscopy amplifiers are used to couple the gamma detector signals to the ADC interface to the PC. Variable gain settings on these amplifiers allow 'zooming' the entire range of the ADC into a desired range of detector energy levels. For example, acquiring data for a gamma energy range of 0-2 MeV would require double the gain as that for 0-4 MeV. However, since the number of channels in the ADC are finite, focusing the entire range of the ADC into a smaller energy range ensures better energy resolution in the detected data. This is important when looking for specific energy peaks from certain elements, which lie close to energy peaks from other elements, as in the case of iron (56Fe at 846.7 keV) and germanium (74Ge at 841.1keV).

*B. Spectral Acquisition Methodology*

Spectral acquisition for samples was done by using SpecTcl to capture two measurable parameters for each gamma count observed: gamma TOF and gamma photon energy. Several scalars associated with the event, including neutron flux, accelerator beam current, and zero-degree monitor counts, were also recorded separately from the spectral data. For tomography, the sample position was recorded by reading the sample manipulator's x,y,z positions at each projection as the sample was translated and rotated. Each projection was then analyzed separately and results were fed to the reconstruction algorithm. Data was recorded until enough counts were observed above background noise.

Recorded data sets could be retrieved and analyzed in both real-time while acquiring data as well as at a later time. Analysis parameters such as TOF windows and detector calibration bias were applied and adjusted in software to allow replaying the experiment with different windows for off-line optimization of these parameters. Spectra were generated using the Xamine display program with different combinations of timing and energy windows applied to the acquired data.

*1) Background Reduction*

Background reduction was performed using three techniques: a TOF background suppression technique [36, 37], a sample-out scan subtraction [37], and finally polynomial curve-fitting for residual background [13-15]. The TOF suppression technique is used to correct for time-uncorrelated background noise from the room and noise generated from the experimental setup. This technique uses a pulsed neutron beam to allow only those gamma photons which appear within a pre-set time window corresponding to the time of flight for a neutron from the source to the sample plus the time of flight for the subsequently emitted gamma from the sample to the detector. The remaining gamma photons are suppressed as 'background noise'. Our implementation of this technique has been described in detail elsewhere [37].

Sample-out subtraction is performed by acquiring data for equal time duration with the sample removed. This gives an estimate of the room background noise originating from factors that are not related to the sample, for example interactions between neutrons and the collimator or sample holder. This data is subtracted from the sample-in data to get an estimate of the spectrum originating from the sample. In this study, as the samples of interest were only the elements present in the tissue, the sample-out scan was acquired by substituting the tissue sample with an equivalent mass of water, i.e. 'removing' only the elements of interest while retaining the neutron scatter properties of hydrogen nuclei in tissue.

Polynomial curve fitting is used to remove residual background due to energy spread from detected gammas in the lower energy channels of the detector. When a high energy gamma photon is detected, while most of its energy is registered at a value close to the actual photon energy, a part of it spreads to lower energy channels in the detector due to

intrinsic detector inefficiency. Hence, a gamma photon detected at energy *E* contributes not only to counts in channel *E* but also to several detector channels ranging from *E* down to zero. As a result, there is a trend of increasing counts in the lower energy channels of the detector. This trend is modeled using a polynomial curve-fit and is subtracted as residual background. An example of this is shown in Fig. 2, which shows the original uncorrected spectrum (light gray), the polynomial curve (dotted black line) and the residual background corrected spectrum (solid black line).

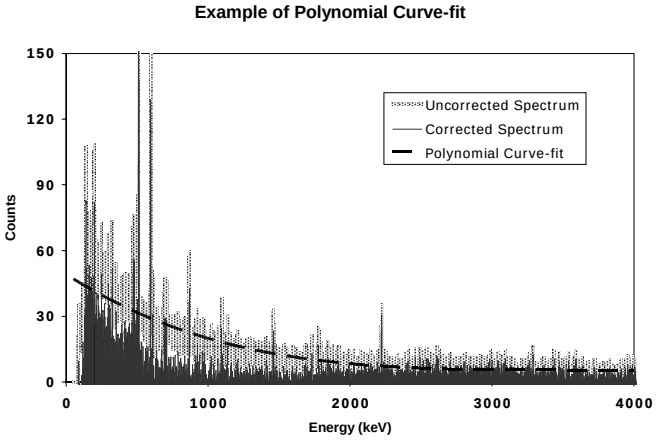


Fig.2. Example of polynomial curve-fitting for residual background correction. The uncorrected spectrum is shown in dotted grey with the polynomial curve overlaid in dotted black. The resulting corrected spectrum is shown in the foreground as a solid black line.

*2) Samples*

Several experiments have been performed to evaluate NSECT's feasibility in detecting elements in biological tissue. Early studies show quantitative information obtained from non-biological blocks of elements such as iron, copper, calcium and carbon [9, 11], as well as mixtures of these elements [10]. Tomographic images have been obtained and reconstructed from a mixed solid phantom of iron and copper [10]. Quantitative analyses have been performed in several physical samples and a bovine liver biological sample [12, 15].

A total of 5 samples were scanned for this study investigating NSECT's ability to detect element concentration changes in human tissue. Samples I and II comprised breast biopsy tissue samples with matched tumors excised from the same patient. Sample I had a benign tumor and Sample II was malignant. Each sample weighed approximately 40g and was scanned for 3 hours with a 6.0 MeV neutron beam while placed in a plastic container. Sample III comprised 40g of distilled water in an identical plastic container, and was used to get an estimate of sample related background originating mainly from hydrogen nuclei in tissue cells. Sample IV was made up of varying concentrations of $^{56}$Fe, $^{23}$Na, $^{39}$K, $^{35}$Cl and $^{37}$Cl in distilled water and was used to determine the lower detection threshold of NSECT. Finally, as none of the above samples were of in-vivo tissue, Sample V comprising a fixed mouse specimen was scanned to demonstrate NSECT's ability in detecting elements from an intact biological specimen. The mouse specimen was prepared as follows. A freshly sacrificed mouse was flushed with saline and then fixed for one week using a 1:10 gadolinium/formalin solution. After flushing the fixed mouse with saline once again, it was enclosed and sealed in a glass tube along with diluted formalin solution. This enclosed specimen was scanned for 95 minutes with a 5.0 MeV monochromatic neutron beam.

Gamma spectra obtained from each sample were normalized against neutron flux monitor counts for the duration of the scan and background corrected.

## III. Results

The results below show background corrected spectra from each of the samples scanned except for Sample III, which was used to estimate background.

Fig. 3 and fig. 4 show background corrected spectra from the benign and malignant tumor samples respectively. Several elements were identified common to both samples. Energy peaks were seen for Ag, Br, Cl, Co, Cr, Cs, Cu, Fe, Mg, Mn, Ni, Rb, Se, Sn, and Zn. Energy peaks were also seen for Ge from the gamma detectors. While several elements were seen to vary in concentration between the two samples, considerable differences were observed for $^{37}$Cl, $^{56}$Fe, $^{58}$Ni, $^{59}$Co, $^{66}$Zn, $^{79}$Br and $^{87}$Rb.

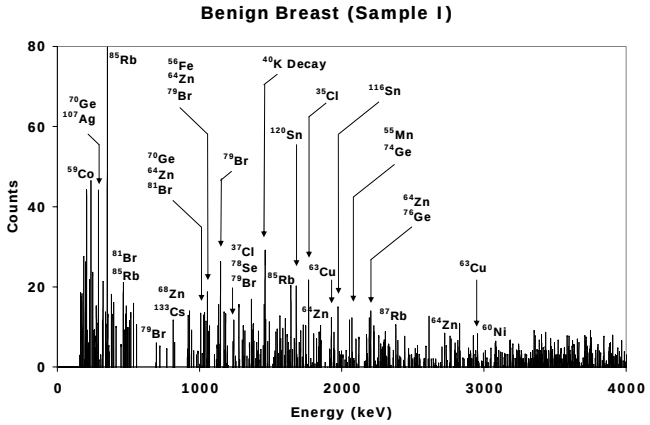


Fig.3. Gamma spectrum from benign breast sample showing energy peaks for several potential elements identified. Gamma peaks are seen for $^{72}$Ge and $^{74}$Ge from the germanium detector. Peaks with multiple potential element matches are labeled accordingly.

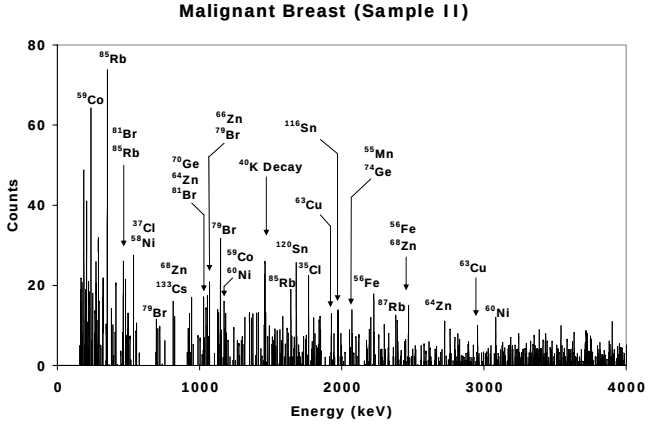

Fig.4. Gamma spectrum from malignant breast sample showing energy peaks for several potential elements identified. Gamma peaks are seen for $^{72}$Ge and $^{74}$Ge from the germanium detector. Peaks with multiple potential element matches are labeled accordingly.

Fig. 5 shows the gamma spectrum from the mixed Fe-Na-K-Cl sample containing 5g Fe, 0.98g Na, 1.31g K, and 2.71g Cl. Peaks were seen for each of the elements present in the sample. Assuming the statistical noise in the system to remain constant, the detection threshold for NSECT was determined to be 0.5g for all four elements, i.e. at least 0.5g of an element would have to be present in the beam to be detected and quantified accurately with a p-value $\leq 0.05$.

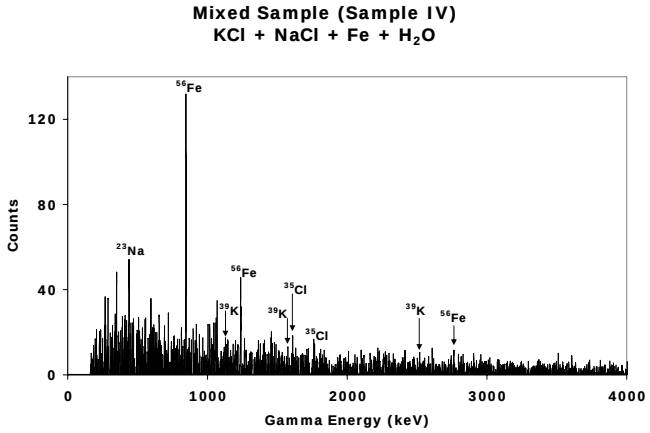


Fig.5. Gamma spectra from a mixed sample of 2.5g KCl, 2.5g NaCl and 5g Fe in 40g $H_2O$. Peaks are seen for each of the elements in the sample.

Fig. 6 shows the gamma spectrum for the fixed mouse specimen. Gamma peaks were observed for several elements expected from the mouse specimen as well as some from materials present in the scanning setup. Energy peaks were identified for $^{12}$C from tissue, $^{40}$Ca from bone, and elements $^{39}$K, $^{27}$Al, $^{37}$Cl, $^{56}$Fe, $^{68}$Zn and $^{25}$Mg which could be present in the specimen. Elements $^{27}$Al and $^{56}$Fe could also be system dependent as many components used to mount the detectors and other hardware were made of aluminum and iron. Peaks were seen for $^{158}$Gd and $^{160}$Gd from the 1:10 gadolinium/formalin fixing solution in the sample, along with peaks from several naturally occurring states in germanium in the HPGe detectors.

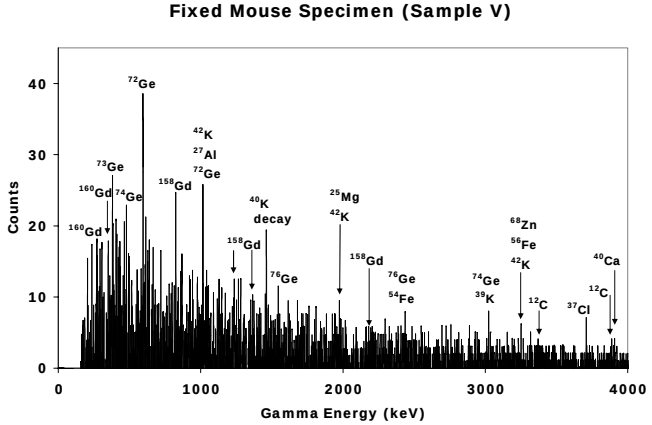


Fig. 6 Gamma spectrum from a formalin fixed mouse specimen showing peaks corresponding to excited states in various elements. Gamma peaks are seen for $^{12}$C (escape peaks), $^{40}$Ca, $^{39}$K, $^{27}$Al, $^{37}$Cl, $^{56}$Fe, $^{68}$Zn and $^{25}$Mg. Gamma peaks are also seen for $^{72}$Ge and $^{74}$Ge from the germanium detector, and $^{158}$Gd and $^{160}$Gd from the fixing solution. Peaks with multiple potential element matches are labeled accordingly

## IV. Discussion

NSECT shows significant promise in developing into a modality capable of detecting breast cancer in very early stages. Results from preliminary scans of breast tissue samples demonstrate its ability in detecting individual elements within breast tissue, may be potential indicators of several disorders including breast cancer. Although the spectra obtained in this study were from excised tissue, results from the whole mouse specimen indicate that element detection is possible for in-vivo tissue without the need for biopsy. The lower detection threshold for accurate quantification of an element was established to be 0.5 grams. This threshold value is much higher than the microgram sensitivity required to detect cancer-indicating trace elements in the breast. At this point element quantification can only be performed for samples with at least 0.5 grams of the target element in the beam. In some cases this may be made possible by using a broad neutron beam to illuminate a larger area of the body. Generally, a significant sensitivity improvement will be required for breast cancer diagnosis. Efforts are under way to improve sensitivity while maintaining the lowest possible dose level delivered to the patient. Using high-flux neutron sources and multiple gamma detectors will increase the overall detection efficiency and reduce scan time, which will both in turn reduce the time-dependent background noise. Optimizing the detector shielding will reduce the sample-related and room-related background, which will increase signal to noise ratio and improve the sensitivity of the system. Increasing the gamma detection efficiency to reduce overall scan time will also reduce the associated patient dose. Neutron and gamma attenuation correction algorithms are being developed and implemented simultaneously to improve sensitivity and detection accuracy [38].

Three background correction techniques were used in this experiment, TOF correction, sample-related background subtraction, and polynomial curve-fitting. The TOF correction technique is used to reduce the time-uncorrelated room background. This room background can also be estimated by acquiring a spectrum from a sample-out scan. Both techniques have been tested and are seen to suppress time-uncorrelated background sufficiently. We prefer to implement the TOF subtraction technique here because not only does it require less time by not having to acquire a separate sample-out scan, but the electronics are also readily available at TUNL. In a clinical environment however, it may be easier to use the sample-out subtraction technique to avoid the added complexity in required hardware.

Using neutrons as the incident radiation leads to significant concerns about patient dose. At our energies of interest (2 MeV to 8 MeV), neutrons are known to damage the body 10 times more than x-rays. However, it takes an immensely smaller number of neutrons to create an NSECT image than x-

rays required to create a mammogram. Hence it is possible to maintain patient dose level at values comparable to other ionizing radiation modalities. Our preliminary experiments suggest that for breast cancer detection, it may be possible to achieve effective patient dose levels of approximately 20 mSv. By increasing the number of detectors and using high-flux neutron sources to reduce scan time, dose levels can potentially be brought down even further, comparable to patient dose from screening mammography. Dose measurements are currently performed through a Geant4 simulation which models the acquisition geometry, neutron beam characteristics and tissue sample data. The simulation is used to count the energy deposited in the tissue sample from which an effective dose equivalent for the organ can be calculated by using the appropriate weighting factors for the organ of interest. For the breast, the weighting factor relative to whole body exposure is 0.05.

NSECT has the potential to detect breast cancer. Its advantage lies in its ability to detect and identify malignant tissue in the breast and generate a two-dimensional image through a single non-invasive in-vivo tomographic scan without the need for breast compression or biopsy. Through the use of portable neutron sources and portable gamma detectors, NSECT can evolve into an easily accessible screening modality and diagnostic technique for breast cancer. Our final goal is to implement a portable, low-dose breast cancer screening system which can detect breast cancer without the need for breast compression or invasive biopsies.

## ACKNOWLEDGMENT

We thank all the members of the Triangle Universities Nuclear Laboratory for their help with data acquisition and the members of Duke Advanced Imaging Laboratories for their help with data analysis. We thank the Center for In-vivo Microscopy at Duke University for providing the fixed mouse specimen.

## REFERENCES

[1] A. Garg, V. Singh, et al., "An elemental correlation study in cancerous and normal breast tissue with successive clinical stages by neutron activation analysis," *Biological Trace Element Research*, vol. 46, pp. 185-202, 1994.

[2] Y. Katoh, T. Sato, and Y. Yamamoto, "Use of instrumental neutron activation analysis to determine concentrations of multiple trace elements in human organs," *Arch. Environ. Health*, vol. Oct, 2003.

[3] G. S. Knight, A. H. Beddoe, S. J. Streat, and G. L. Hill, "Body composition of two human cadavers by neutron activation and chemical analysis," *Am J Physiol Endocrinol Metab*, vol. 250, pp. E179-185, 1986.

[4] M. Yukawa, M. Suzuki-Yasumoto, and K. Amano, Terai, M., "Distribution of trace elements in the human body determined by neutron activation analysis," *Arch. Environ. Health*, vol. 35, pp. 36-44, 1980.

[5] A. Danielsen, Steinnes, E., "A study of some selected trace elements in normal and cancerous tissue by neutron activation analysis," *J. Nuclear Med.*, vol. 11, pp. 260-264, 1970.

[6] K. H. Ng, Bradley, D.A., Looi, L.M., Seman Mahmood, C., Khalik Wood, A., "Differentiation of elemental composition of normal and malignant breast tissue by instrumental neutron activation analysis," *Appl. Radiat. Isot.*, vol. 44, pp. 511-516, 1993.

[7] G. V. Iyengar, K. Kasperek, and L. E. Feinendegen, "Determination of certain bulk and trace elements in the bovine liver matrix using neutron activation analysis," *Phys. Med. Biol*, vol. 23, pp. 66-76, 1978.

[8] W. E. Kollmer, P. Schramel, and K. Samsal, "Simultaneous determination of nine elements in some tissues of the rat using neutron activation analysis," *Phys. Med. Biol*, vol. 17, pp. 555-562, 1972.

[9] C. E. Floyd, J. E. Bender, A. C. Sharma, A. J. Kapadia, J. Q. Xia, B. P. Harrawood, G. D. Tourassi, J. Y. Lo, A. S. Crowell, and C. R. Howell, "Introduction to neutron stimulated emission computed tomography," *Physics in Medicine and Biology*, vol. 51, pp. 3375-3390, 2006.

[10] C. E. Floyd, J. E. Bender, A. C. Sharma, A. J. Kapadia, J. Q. Xia, B. P. Harrawood, G. D. Tourassi, J. Y. Lo, A. S. Crowell, and C. R. Howell, "Neutron Stimulated Emission Computed Tomography of a Multi-Element Phantom," *IEEE Trans Med Imag (submitted)*, 2006.

[11] C. E. Floyd, C. R. Howell, B. P. Harrawood, A. S. Crowell, A. J. Kapadia, R. Macri, J. Q. Xia, R. Pedroni, J. Bowsher, M. R. Kiser, G. D. Tourassi, W. Tornow, and R. Walter, "Neutron Stimulated Emission Computed Tomography of Stable Isotopes," *Proceedings of SPIE Medical Imaging 2004*, vol. 5368, pp. 248-254.

[12] A. J. Kapadia, C. E. Floyd, J. E. Bender, C. R. Howell, A. S. Crowell, and M. R. Kiser, "Non-invasive quantification of iron 56-Fe in beef liver using neutron stimulated emission computed tomography," *Proceedings of IEEE Nuclear Science Symposium, Medical Imaging Conference 2005*, vol. 4, pp. 2232-2234.

[13] A. J. Kapadia, A. C. Sharma, G. D. Tourassi, J. E. Bender, C. R. Howell, A. S. Crowell, M. R. Kiser, and C. E. Floyd, "Neutron Spectroscopy of Mouse Using Neutron Stimulated Emission Computed Tomography (NSECT)," *Proceedings of IEEE Nuclear Science Symposium, Medical Imaging Conference (in press) 2006*.

[14] A. J. Kapadia, A. C. Sharma, G. D. Tourassi, J. E. Bender, C. R. Howell, A. S. Crowell, M. R. Kiser, and C. E. Floyd, "Neutron Stimulated Emission Computed Tomography (NSECT) for Early Detection of Breast Cancer," *Proceedings of IEEE Nuclear Science Symposium, Medical Imaging Conference (in press) 2006*.

[15] A. J. Kapadia, A. C. Sharma, G. D. Tourassi, J. E. Bender, C. R. Howell, A. S. Crowell, M. R. Kiser, and C. E. Floyd, "Non-Invasive Estimation of Potassium (39K) in Bovine Liver Using Neutron Stimulated Emission Computed Tomography (NSECT)," *Proceedings of IEEE Nuclear Science Symposium, Medical Imaging Conference (in press) 2006*.

[16] J. E. Bender, C. E. Floyd, B. P. Harrawood, A. J. Kapadia, A. C. Sharma, and J. L. Jesneck, "The effect of detector resolution for quantitative analysis of neutron stimulated emission computed tomography," *Proceedings of SPIE Medical Imaging 2006*, vol. 6142, pp. 1597-1605.

[17] A. C. Sharma, G. D. Tourassi, A. J. Kapadia, J. E. Bender, J. Q. Xia, B. P. Harrawood, A. S. Crowell, M. R. Kiser, C. R. Howell, and C. E. Floyd, "Development of a High-Energy Gamma Camera for Use with NSECT Imaging of the Breast," *Proceedings of IEEE Nuclear Science Symposium, Medical Imaging Conference (in press) 2006*.

[18] K. H. Ng, Bradley, D.A., Looi, L.M., "Elevated trace element concentrations in malignant breast tissues," *British Journal of Radiology*, vol. 70, pp. 375-382, 1997.

[19] S. Rizk and H. Sky-Peck, "Comparison between concentrations of trace elements in normal and neoplastic human breast tissue," *Cancer Research*, vol. 44, pp. 5390-5394, 1984.

[20] A. Schwartz and R. Fink, "Trace Elements in Normal and Malignant Human Breast Tissue," *Surgery*, vol. 76, pp. 325-329, 1974.

[21] R. Engelhardt, J. H. Langkowski, R. Fischer, P. Nielsen, H. Kooijman, H. C. Heinrich, and E. Bucheler, "Liver iron quantification: studies in aqueous iron solutions, iron overloaded rats, and patients with hereditary hemochromatosis," *Magn Reson Imaging*, vol. 12, pp. 999-1007, 1994.

[22] J. P. Villeneuve, M. Bilodeau, R. Lepage, J. Cote, and M. Lefebvre, "Variability in hepatic iron concentration measurement from needle-biopsy specimens," *J Hepatol*, vol. 25, pp. 172-7, 1996.

[23] J. M. Alustiza, J. Artetxe, A. Castiella, C. Agirre, J. I. Emparanza, P. Otazua, M. Garcia-Bengoechea, J. Barrio, F. Mujica, and J. A.

Recondo, "MR quantification of hepatic iron concentration," *Radiology*, vol. 230, pp. 479-84, 2004.
[24] L. W. Powell, "Diagnosis of hemochromatosis," *Semin Gastrointest Dis*, vol. 13, pp. 80-8, 2002.
[25] S. R. Hollan, "Transfusion-associated iron overload," *Curr Opin Hematol*, vol. 4, pp. 436-41, 1997.
[26] S. Joffe, "Hemochromatosis," N. Lamki, B. D. C. U. P. Schmiedl, R. M. Krasny, and J. Karani, Eds., 2005.
[27] L. Powell, "Hemochromatosis," in *Harrison's Principals of Internal Medicine*, vol. 2, D. Kasper, Fawci, AS, Longo, DL, Braunwald, E, Hauser, SL, Jameson, JL, Ed., 16 ed. NY: McGraw Hill, 2005, pp. 2298-2303.
[28] G. Brewer, "Wilson Disease," in *Harrison's Principals of Internal Medicine*, vol. 2, D. Kasper, Fawci, AS, Longo, DL, Braunwald, E, Hauser, SL, Jameson, JL, Ed., 16 ed. NY: McGraw Hill, 2005, pp. 2313-2315.
[29] A. P. Dempster, N. M. Laird, and D. B. Rubin, "Maximum likelihood from incomplete data via the EM algorithm," *J R Stat Soc Series B*, vol. 39, pp. 1-38, 1977.
[30] R. Sundberg, "Maximum likelihood theory for incomplete data from an exponential family," *Scand J Stat*, vol. 1, pp. 49-58, 1974.
[31] L. Shepp and Y. Vardi, "Maximum likelihood reconstruction for emission tomography," *IEEE Trans. Med. Imag.*, vol. MI-1, pp. 113-122, Oct.1982.
[32] NCI, "A Snapshot of Breast Cancer," National Cancer Institute 2006.
[33] ACS, "Cancer Facts and Figures 2006," American Cancer Society, Atlanta 2006 2006.
[34] D. B. Kopans, "The Positive Predictive Value of Mammography," *American Journal of Roentgenology*, vol. 158, pp. 521-526, 1992.
[35] H. Mussalo-Rauhamaa, S. Piepponen, J. Lehto, R. Kauppila, and O. Auvinen, "Cu, Zn, Se and Mg concentrations in breast fat of Finnish breast cancer patients and healthy controls," *Trace Elements in Medicine*, vol. 10, pp. 13-15, 1993.
[36] P. Håkansson, "An introduction to the time-of-flight technique," *Braz. J. Phys.*, vol. 29, pp. 422-427, 1999.
[37] C. E. Floyd, A. C. Sharma, J. E. Bender, A. J. Kapadia, J. Q. Xia, B. P. Harrawood, G. D. Tourassi, J. Y. Lo, M. R. Kiser, A. S. Crowell, R. S. Pedroni, R. A. Macri, S. Tajima, and C. R. Howell, "Neutron Stimulated Emission Computed Tomography: Background Corrections," *Nuclear Instruments and Methods in Physics Research Section B (accepted)*, 2006.
[38] A. J. Kapadia and C. E. Floyd, "An attenuation correction technique to correct for neutron and gamma attenuation in the reconstructed image of a neutron stimulated emission computed tomography (NSECT) system," *Proceedings of SPIE Medical Imaging 2005*, vol. 5745, pp. 737-743.

# Breast cancer detection using Neutron Stimulated Emission Computed Tomography: prominent elements and dose requirements

Janelle E. Bender[1,2], Anuj J. Kapadia[1,2], Amy C. Sharma[1,2], Georgia D. Tourassi[2], Brian P. Harrawood[2], and Carey E. Floyd, Jr.[1,2]

[1]*Department of Biomedical Engineering, Duke University, Durham, North Carolina 27708*

[2]*Duke Advanced Imaging Laboratories, Department of Radiology, Duke University, Durham, North Carolina 27708*

(Received

Neutron Stimulated Emission Computed Tomography (NSECT) is being developed to non-invasively determine concentrations of trace elements in biological tissue. Studies have shown prominent differences in the trace element concentration of normal and malignant breast tissue. NSECT has the potential to detect these differences and diagnose malignancy with high accuracy with dose comparable to that of a single mammogram. In this study, NSECT imaging was simulated for normal and malignant human breast tissue samples to determine the significance of individual elements in determining malignancy. The normal and malignant models were designed with different elemental compositions, and each was scanned spectroscopically using a simulated 2.5 MeV neutron beam. The number of incident neutrons was varied from 0.5 million to 10 million neutrons. The resulting gamma spectra were evaluated through Receiver Operating Characteristic (ROC) analysis to determine which trace elements were prominent enough to be considered markers for breast cancer detection. Three elements ($^{133}$Cs, $^{81}$Br, and $^{87}$Rb) at four energy levels were shown to be promising features for breast cancer detection with an area under the ROC curve ($A_Z$) above 0.85. Two of these elements – $^{81}$Br at 1109keV and $^{87}$Rb at 1338 keV – achieved perfect classification at 10 million incident neutrons and could be detected with as low as 1 million incident neutrons. Patient dose was calculated for each gamma spectrum obtained and was found to range from 0.05 mSv for 0.5 million neutrons to 0.112 mSv for 10 million neutrons. This simulation demonstrates that NSECT has the potential

to non-invasively detect breast cancer at a fraction of the dose of a mammogram, through 4 prominent trace elements.

Key Words: Monte Carlo, neutrons, tomography, gamma-ray spectroscopy, breast cancer

## I. INTRODUCTION

NEUTRON Stimulated Emission Computed Tomography (NSECT) is a new technique being developed to non-invasively image the elemental composition of tissues within the human body. When a high-energy fast neutron (2.5-5 MeV) inelastically scatters off an atomic nucleus, the nucleus is excited, and a gamma ray is emitted. The energy of the gamma is characteristic of the atomic nucleus with which it interacted. By analyzing the energy levels of the emitted gammas when a sample is bombarded with many neutrons, the elemental composition can be determined.

Many studies have shown there to be a difference in the elemental composition of normal, benign, and malignant tissue in humans for a large variety of cancers, including breast cancer[1-5], prostate cancer[6], and glioblastoma multiforme[7]. To determine compositional differences, these studies have required invasive methods, such as biopsy. The NSECT technique has the potential to measure these differences non-invasively, *in vivo*, with a dose lower than that of standard two-view mammography[8].

NSECT has the potential to evolve into a powerful, low-dose screening or diagnostic technology for breast cancer. One study showed that there were elevated levels of Fe, Cu, Zn, and K in human breast tumor tissue when compared to healthy breast tissue[9]. This study utilized x-ray fluorescence (XRF) emitted from the elements in *ex vivo* breast tissue samples with a synchrotron-based system. In XRF, tissue samples remain intact and there is direct quantification of the elements, but the system necessitates the use of biopsied tissue. Another study found that malignant breast tissue has significantly higher concentrations of 12 trace elements (Al, Br, Ca, Cl, Co, Cs, Fe, K, Mn, Na, Rb, and Zn) when compared to adjacent normal breast tissue[10]. This study employed Neutron Activation Analysis (NAA), an invasive and destructive technique, which typically involves freeze-drying of excised breast tissue[11]. Because measurements were made on dried tissue, a wet-to-dry ratio had to be implemented in order to convert values to ones relevant in intact breast tissue. Additionally, NAA renders the interrogated sample

radioactive. While NAA is high in sensitivity, it lacks the ability to be translated to a low-dose *in vivo* method.

We present NSECT as an imaging modality that has the potential to be translated to the clinic, due to its non-invasive nature. We have already demonstrated spectroscopic acquisition over a broad energy range that encompasses many elements of interest for biological imaging[12]. The present study uses Monte Carlo simulations and Receiver Operating Characteristic analysis to investigate the performance of different elements in differentiating malignant and normal breast tissue at clinically acceptable dose levels. Before evaluations can be performed on anatomic models of the breast containing lesions and nodules with trace element concentration differences, it must be tested whether it is possible to detect any trace element concentration changes in the presence of all the scatter noise generated by the tissue. Hence this study uses models of bulk breast tissue to investigate the feasibility of NSECT in trace element quantification to detect breast cancer.

## II. METHODS

### 2.1. Monte Carlo simulations

Monte Carlo simulations were designed using Geant4[13]. Bulk breast tissue was modeled as an ellipsoid 10 cm x 6 cm x 5 cm. Two high-purity germanium (HPGe) detectors[14] with 12 cm diameter and 5cm height flanked the breast tissue and were offset by 11.6 cm (see Figure 1).

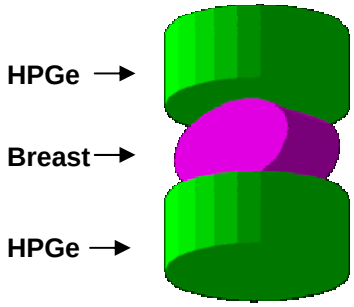


**Figure 1: Geant4 setup. Two HPGe detectors flank the breast tissue. Incoming neutrons strike at the face of the breast.**

The interaction of fast neutrons (2.5 MeV) incident upon bulk breast tissue was modeled in Geant4. In the case of neutron inelastic scattering, the nucleus is excited and emits a characteristic gamma ray. Geant4 determines the direction of the emitted gamma, which may then be deposited in one of the two gamma detectors. The gamma ray energy deposited in each detector was tabulated to form a gamma spectrum

showing energy levels and corresponding gamma counts, or intensity. The energy was then matched to the element with which the neutron had an interaction, which was deduced using a look-up table from the Evaluated Nuclear Data Files (ENDF) database[15].

Breast tissue was modeled as either being normal or malignant, with elemental compositions[10] as seen in Table 1. The normal breast tissue had a density of 0.93 g/cm$^3$, and the malignant breast tissue had a density of 1.058 g/cm$^3$, which correspond to adipose tissue and masses, respectively[16]. Over 99% of the breast tissue is comprised of O, C, H, and N, but the neutron energy of 2.5MeV that we used was too low to excite O, C, and N. We did see neutron capture on H, which was easily distinguishable. The remainder of the peaks can be attributed to excitations from the trace elements, which are of interest because they can be linked to malignancy.

| | **Normal (%)** | **Malignant (%)** |
|---|---|---|
| **Oxygen** | 61.429 | 61.429 |
| **Carbon** | 22.857 | 22.857 |
| **Hydrogen** | 12.649 | 12.510 |
| **Nitrogen** | 2.571 | 2.571 |
| **Chlorine** | 1.98E-2 | 2.15E-2 |
| **Sodium** | 1.85E-2 | 2E-2 |
| **Potassium** | 8.94E-2 | 1.96E-2 |
| **Iron** | 9.8E-3 | 7.85E-3 |
| **Calcium** | 8.29E-3 | 1.13E-2 |
| **Zinc** | 1.17E-3 | 1.14E-3 |
| **Bromine** | 7.07E-4 | 6.55E-4 |
| **Aluminum** | 6.67E-4 | 5.7E-4 |
| **Rubidium** | 5.98E-4 | 5.84E-4 |
| **Manganese** | 3.88E-5 | 3.16E-5 |
| **Cobalt** | 2.06E-5 | 1.98E-5 |
| **Cesium** | 3.27E-7 | 3.6E-7 |

**Table 1: Breast tissue composition for normal and malignant models. The percentages were calculated by first converting dry weights to wet weights.**

Ten simulations of 10 million incident neutrons were run on both the normal and malignant models. For each simulation, a new random seed was generated. Additionally, runs of 0.5 million, 1 million, 2

million, 3 million, and 5 million incident neutrons were produced by using the desired number of events from the corresponding runs of 10 million. This yielded a total of 60 spectral scans per tissue type.

### 2.2. Peak-identification algorithm

For each output file, the energies in keV were tabulated to yield spectra of gamma energy and corresponding gamma intensity. The first task was to determine whether or not the intensity at a specific energy could be considered a peak in the spectrum. To be called a peak, three criterions had to be met: (1) the peak had to exceed a set minimum count level, (2) the peak had to be larger than all other peaks in a specified window, and (3) the peak energy had to match to one of the elements in the breast tissue model. The minimum peak height was set to be 40 counts, which exceeded the underlying noise throughout the energy range (0-2500 keV). An iterative technique was used to optimize the window width. Window widths were varied from ±2 to ±20 keV, and the number of detected peaks was correlated with the number of expected peaks in the simulated spectra. The best results were seen for a window width of ±10 keV. The element that the characteristic energy represented was determined using the ENDF tables. Figure 2 shows an example of the peak-identification technique for one of the runs of 10 million incident neutrons. The circles mark the energies that fit the first two criteria, and the labels note the corresponding element if the peak fit the third criterion.

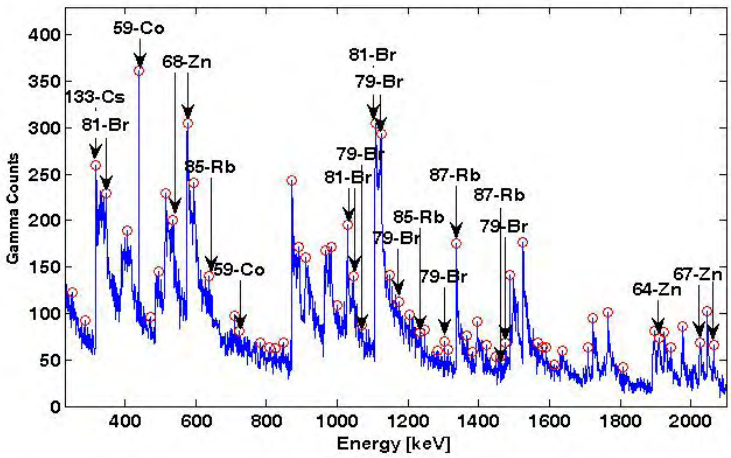


**Figure 2: Spectrum of 10 million incident neutrons. The circles represent energy levels at which the counts exceeded 40 and at which the counts exceeded all counts in a ±10 keV window. Labels are provided for those peaks that matched elements found in the modeled breast tissue.**

The process of peak-identification was performed on output files from the ten normal and ten malignant simulations for the 10 million incident neutrons level. Peak-identification was performed only for the highest incident neutron level as a best-case scenario to identify peaks that could be detected in the breast tissue.

125

**2.3. ROC analysis**

The detectability index was the area under the binormal ROC curves, or $A_z$. The significance of a peak at lower levels of incident neutrons was determined by monitoring the degradation in the area under the ROC curve for that peak as the number of incident neutrons was reduced. In order for a specific energy
130 peak to be used in the ROC analysis, more than 5 of the 10 files for each case (normal or malignant) had to register the given peak. The purpose of this criterion was to focus only on the peaks found in the majority of each tissue model. The ROC analysis was conducted for each of the matched energy levels using the software, ROCKIT[17]. ROCKIT uses maximum likelihood estimation to fit a binormal ROC curve to continuously-distributed data and/or categorical data[18]. There were two categories for the ROC analysis:
135 "actually-negative" and "actually-positive," which respectively correspond to normal and malignant status.

Because ROC analysis was performed on a small sample size (n=20), it was expected that $A_z$ estimates would have a relatively large variance. To ensure that the peaks selected were truly powerful, we applied a minimum threshold of $A_z = 0.85$.

140 **2.4. Dose calculations**

One of the primary concerns with any potential clinical imaging technique is the absorbed patient dose. The dose was calculated for each run as follows. Using a separate Monte Carlo simulation, the average energy deposited in the breast tissue per 2.5 MeV incident neutron was determined to be 1.4 MeV[8]. As the neutrons irradiated a 10 $cm^3$ volume of tissue, the total irradiated mass could be calculated using the
145 density of the breast tissue. This was then converted into the absorbed dose, $D_{T,R}$, in a tissue or organ T due to radiation R, measured in J/kg or Sv. The equivalent dose, $H_{T,R}$, was then calculated as in Equation 1, where $\omega_R$ is the radiation weighting factor. For neutrons with energy between 2 MeV to 20 MeV, $\omega_R$ =

10[19]. The effective dose, E, to the breast tissue was calculated using Equation 2, where $\omega_T$ is the tissue weighting factor, which for breast is equal to 0.05[20].

$$H_{T,R} = \omega_R \cdot D_{T,R} \quad (1)$$

$$E = \omega_T \cdot H_{T,R} \quad (2)$$

Using the method described above, the effective dose was estimated to be 1.12E-8 mSv/neutron.

## III. RESULTS

For the ten normal tissue runs of 10 million incident neutrons, 27 energy levels were found to be peaks in over half of the runs. For the ten corresponding malignant runs, 26 energy levels were designated as peaks in over half of the runs. These energy levels were queried in the ENDF tables; eight levels in the normal model and eight levels in the malignant model corresponded to elements from the breast tissue model. Five of these energy peaks were common to both the normal and malignant models, suggesting that they robustly appear in the majority of tissue samples from each population. Table 2 summarizes the energy levels and the corresponding number of matches for normal and malignant models.

| | | Normal | Malignant |
|---|---|---|---|
| **319keV** | **$^{133}$Cs** | ✓ (10) | ✓ (9) |
| **439keV** | **$^{59}$Co** | ✓ (10) | ✓ (10) |
| **1029keV** | **$^{81}$Br** | ✓ (10) | ✓ (10) |
| **1109keV** | **$^{81}$Br** | ✓ (9) | (5) |
| **1191keV** | **$^{79}$Br** | (4) | ✓ (6) |
| **1204keV** | **$^{67}$Zn** | ✓ (6) | (4) |
| **1338keV** | **$^{87}$Rb** | ✓ (6) | ✓ (6) |
| **1476keV** | **$^{79}$Br** | ✓ (7) | (5) |
| **1697keV** | **$^{41}$K** | (3) | ✓ (6) |
| **1973keV** | **$^{67}$Zn** | (5) | ✓ (7) |
| **2065keV** | **$^{67}$Zn** | ✓ (6) | ✓ (6) |

**Table 2: Number of energy levels and corresponding elemental matches for both the normal and malignant models. A checkmark indicates the matches were found in over half of the output files. The number in parentheses is the number of output files which had a match, out of the total ten files.**

A total of 11 energy levels were found to be peaks in over half the runs in either tissue model using 10 million incident neutrons. Only these peaks were further analyzed with ROC at the six different incident neutron levels considered in this simulation. ROC analysis on the 66 total energy level/incident neutron combinations yielded 16 total combinations with ROC $A_z > 0.85$. As seen in Table 3, each of these combinations corresponded to one of four separate energy levels – 319 keV, 1029 keV, 1109 keV, and 1338 keV, representing elements $^{133}$Cs, $^{81}$Br, $^{81}$Br, and $^{87}$Rb, respectively. Aside from 1109 keV, all these prominent energy levels satisfied the condition of element matching in over five of ten normal and malignant output files. For 1109 keV, this condition was satisfied only for the normal tissue model. Two combinations – 1109 keV and 1338 keV with 10 million incident neutrons – yielded a perfect $A_z$ value of 1.00. Figure 3 summarizes the mean and standard deviation of the ROC $A_z$ values as a function of number of neutrons for all energy levels.

| keV | Millions of incident neutrons | | | | | |
|---|---|---|---|---|---|---|
| | **0.5** | **1** | **2** | **3** | **5** | **10** |
| **319 $^{133}$Cs** | 0.60± 0.13 | 0.78± 0.10 | **0.88± 0.09** | **0.92± 0.06** | **0.92± 0.07** | **0.91± 0.07** |
| 439 $^{59}$Co | 0.45± 0.13 | 0.56± 0.14 | 0.59± 0.13 | 0.70± 0.12 | 0.66± 0.12 | 0.65± 0.12 |
| **1029 $^{81}$Br** | 0.35± 0.13 | 0.46± 0.13 | 0.49± 0.13 | 0.67± 0.12 | **0.93± 0.06** | **0.98± 0.03** |
| **1109 $^{81}$Br** | 0.62± 0.13 | **0.91± 0.07** | **0.96± 0.04** | **0.97± 0.05** | **0.95± 0.05** | **1.00** |
| 1191 $^{79}$Br | 0.61± 0.13 | 0.61± 0.13 | 0.72± 0.11 | 0.73± 0.11 | 0.63± 0.13 | 0.71± 0.12 |
| 1204 $^{67}$Zn | 0.56± 0.14 | 0.74± 0.13 | 0.60± 0.13 | 0.57± 0.13 | 0.65± 0.12 | 0.82± 0.10 |
| **1338 $^{87}$Rb** | 0.70± 0.13 | **0.91± 0.07** | **0.87± 0.09** | **0.93± 0.06** | **0.92± 0.06** | **1.00** |
| 1476 $^{79}$Br | 0.60± 0.13 | 0.61± 0.13 | 0.70± 0.12 | 0.69± 0.12 | 0.65± 0.12 | 0.81± 0.10 |
| 1697 $^{41}$K | 0.47± 0.13 | 0.31± 0.12 | 0.36± 0.12 | 0.49± 0.13 | 0.61± 0.13 | 0.63± 0.12 |
| 1973 $^{67}$Zn | 0.36± 0.14 | 0.32± 0.12 | 0.57± 0.13 | 0.53± 0.13 | 0.74± 0.12 | 0.80± 0.10 |
| 2065 $^{67}$Zn | 0.41± 0.13 | 0.46± 0.13 | 0.51± 0.13 | 0.43± 0.13 | 0.40± 0.13 | 0.67± 0.12 |

**Table 3: Elements and corresponding average and standard error for ROC Az values obtained from ROCKIT software. The values in bold are above the significance threshold of Az = 0.85 and are considered significant. The significant error ranged from 0.03 to 0.14.**

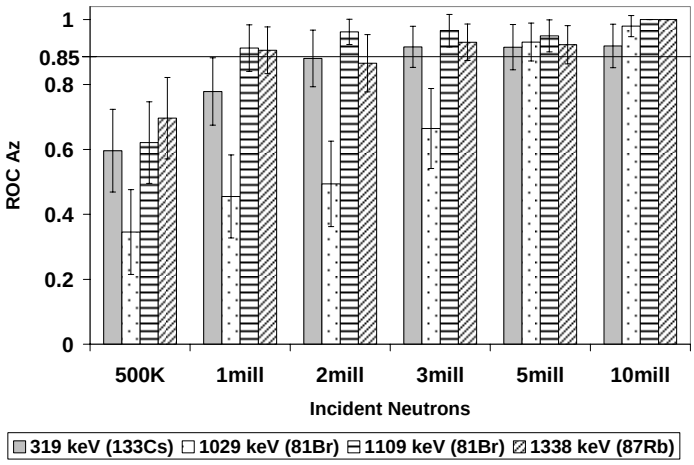


**Figure 3: ROC $A_z$ for the prominent energy levels over all incident neutron count levels. The horizontal line at 0.85 marks the cut-off for prominence.**

No prominent elements were found at the lowest incident neutron level (0.5 million), but $^{81}$Br at 1109 keV and $^{87}$Rb at 1338 keV were found to be significant at the second lowest neutron level (1 million). It should be noted that the elements that were prominent with neutron flux of 1 million incident neutrons were the ones that achieved perfection with 10 million incident neutrons. Figure 4 shows the summation of all normal and malignant runs for 10 million incident neutrons and indicates the peaks which were found to be prominent in the ROC analysis.

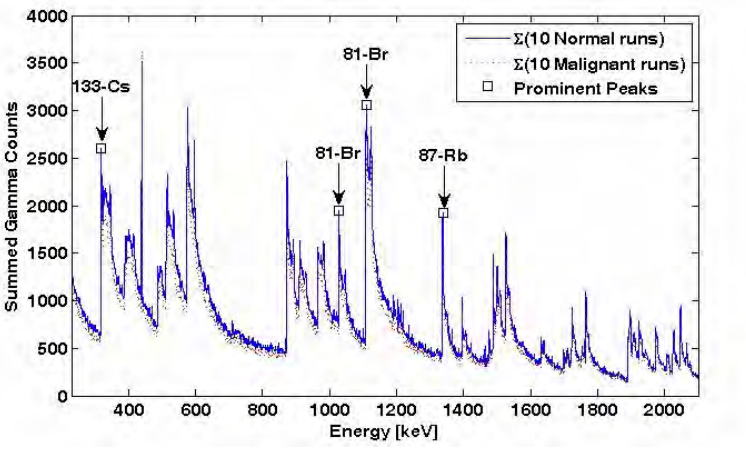


**Figure 4: The ten normal and ten malignant spectra of 10 million incident neutrons were summed. The squares mark the energy levels found to be highly discriminatory in the ROC analysis.**

The dose values calculated for the neutron count levels which yielded prominent elements are summarized in Table 4. For 1 million neutrons, the total dose to the volume of breast tissue that was irradiated was only 0.0112 mSv, which is approximately 0.5% of the mean glandular tissue dose reported for cranio-caudal and medio-lateral-oblique views in mammography[21]. Even when the number of incident neutrons is maximized to 10 million, the dose to the breast tissue is only approximately 5% of that of screening mammography[21].

| Millions of incident neutrons | Corresponding dose to breast |
|---|---|
| 1 | 0.0112 mSv |
| 2 | 0.0224 mSv |
| 3 | 0.0336 mSv |
| 5 | 0.056 mSv |
| 10 | 0.112 mSv |

**Table 4: Calculated effective dose for the levels of incident neutrons that produced prominent elements.**

## IV. DISCUSSION

This simulation study demonstrates NSECT's feasibility to detect differences in the concentration of trace elements that indicate cancer in breast tissue. We have demonstrated the ability to see peaks corresponding to elements in both the normal and malignant bulk breast tissue model. The results indicate that three elements – $^{133}$Cs, $^{81}$Br, and $^{87}$Rb are prominent in differentiating normal from malignant tissue at neutron flux values corresponding to clinically relevant dose levels. Two of these elements achieved perfect classification at 10 million neutrons, and were able to differentiate normal and malignant tissue at a neutron flux as low as 1 million neutrons. As low neutron flux directly implies low dose, these elements are vital for a low-dose clinical implementation of NSECT for breast cancer detection. Further, the ability of these elements in differentiating normal and malignant tissue suggests that NSECT has the potential to develop into a clinical breast cancer screening modality.

The breast in this study was modeled as a bulk section of malignant or normal breast tissue. This was done to test the feasibility of NSECT to detect breast cancer markers in malignant tissue and determine which marker elements are most indicative of cancer. As this feasibility has now been demonstrated, a

logical extension to this study will be to model the anatomy of the normal and malignant breast more accurately to investigate the feasibility of detecting element changes within tumors.

Dose calculated in this study indicates that the dose from an NSECT scan for cancer detection is only a fraction of the dose delivered from a screening mammogram. The ROC analysis results suggest that cancer detection can be performed with a dose of 0.0112 mSv (1 million incident neutrons). Even for the highest neutron flux used (10 million), the dose was calculated as 0.112 mSv, which is considerably lower than screening mammography.

The dose value obtained in this study is calculated for a model of the breast that does not account for sources of background which would otherwise be present in the clinical scanning environment. Before translating this technique to the clinic, an expansion of this study is required to determine the performance when noise is added into the signal. Simulation experiments to model the sources of noise in a clinical environment are currently underway. This study assumes a relatively clean, low-noise signal in detecting an element peak, which results in a low dose estimate. The presence of noise in the system will raise the detection threshold, requiring a larger total concentration of the element for successful detection. Experiments to determine the detection threshold of NSECT in both simulation and clinical environments are being conducted.

From a detection point of view, a logical extension of this study is to develop a fusion classifier to test whether combining elements could be used to detect differences in normal and malignant breast tissue with greater accuracy at lower neutron fluxes. Another extension would be to perform the same set of simulations using a benign breast tissue model to test NSECT's ability to distinguish malignant from benign breast, which is of clinical interest diagnostically. We are encouraged because our current dose estimate is only a fraction of a standard mammography dose. Thus, there is plenty of room to increase the dosage to overcome noise and still conduct an NSECT scan that is within clinically acceptable dose limits.

**ACKNOWLEDGEMENTS**

This work was supported by the NIH/NCI grant 1-R21-CA106873-01 and in part by Department of Defense (Breast Cancer Research Program) under award number W81XWH-06-1-0484 and by NIH Training grant no. 1-T32-EB001040.

Electronic mail: jeb9@duke.edu

[1]Schwartz, A. and R. Fink, "Trace Elements in Normal and Malignant Human Breast Tissue," Surgery **76**, 325-329 (1974).

[2]Ng, K.H., Bradley, D.A., Looi, L.M., Seman Mahmood, C., Khalik Wood, A., "Differentiation of elemental composition of normal and malignant breast tissue by instrumental neutron activation analysis," Appl. Radiat. Isot. **44**(3), 511-516 (1993).

[3]Rizk, S. and H. Sky-Peck, "Comparison between concentrations of trace elements in normal and neoplastic human breast tissue," Cancer Research **44**, 5390-5394 (1984).

[4]Mussalo-Rauhamaa, H., et al., "Cu, Zn, Se and Mg concentrations in breast fat of Finnish breast cancer patients and healthy controls," Trace Elements in Medicine **10**, 13-15 (1993).

[5]Garg, A., V. Singh, et al., "An elemental correlation study in cancerous and normal breast tissue with successive clinical stages by neutron activation analysis," Biological Trace Element Research **46**, 185-202 (1994).

[6]Yaman, M., et al., "Comparison of trace metal concentrations in malign and benign human prostate." J. Med. Chem. **48**, 630-634 (2005).

[7]Andrasi, E., et al., "Concentration of elements in human brain: glioblastoma multiforme," Sci. Total Env. **139-140**, 399-402 (1993).

[8]Floyd, C.E., et al. "Breast cancer diagnosis using neutron stimulated emission computed tomography: dose and count requirements" in *Medical Imaging 2006: Physics of Medical Imaging*, San Diego, CA, USA: SPIE (2006).

[9]Geraki, K., Farquharson, and M.J., Bradley, D.A., "X-ray fluorescence and energy dispersive x-ray diffraction for the quantification of elemental concentrations in breast tissue" Phys. Med. Biol. **49**, 99-110 (2004).

[10]Ng, K.H., Bradley, D.A., Looi, L.M., "Elevated trace element concentrations in malignant breast tissues," British Journal of Radiology **70**, 375-382 (1997).

[11]Sansoni, B. and Iyengar, V., "Sampling and Sample Preparation Methods for the Analysis of Trace Elements in Biological Materials," Jül-Spez-13, Report KFA Jülich, ISSN 0343–7639, (1978).

[12]Floyd, C.E., et al., "Introduction to neutron stimulated emission computed tomography," Phys. Med. Biol. **51**, 3375-3390 (2006).

[13]CERN. *Geant4*. [cited; Available from: wwwinfo.cern.ch/asd/**geant4**/**geant4**.html.

[14]Bender, J.E., et al, "The effect of detector resolution for quantitative analysis of neutron stimulated emission computed tomography" i n *Medical Imaging 2006: Physics of Medical Imaging*, San Diego, CA, USA: SPIE (2006).

[15]Cross Section Evaluation Working Group, ENDEIB-VI Summary Documentation, Report BNL-NCS-17541 (ENDF-201), edited by P.F. Rose, National Nuclear Data Center, Brookhaven National Laboratory, Upton, NY, USA, (1991).

[16]Ullman, G., et al., "Implementation of pathologies in the Monte Carlo model in chest and breast imaging," Report 94 (ISSN 11-2-1799, 2003).

[17]Metz, C.E. *ROC analysis software - ROCKIT*. [cited; Available from: http://www.radiology.uchicago.edu/krl/KRL_ROC/software_index.htm.

[18]Metz, C.E., B.A. Herman, and J.H. Shen, "Maximum likelihood estimation of receiver operating characteristic (ROC) curves from continuously-distributed data," Stat Med **17**(9), 1033-53 (1998).

[19]Turner, J.E., *Atoms, Radiation, and Radiation Protection*, 2nd ed. (John Wiley & Sons, Inc., New York, 1995).

[20]International Commission on Radiological Protection, *1990 recommendations of the International Commission on Radiological Protection*, ICRP Publication 60 (Oxford: Pergamon Press, 1991).

[21]Law, J., "The development of mammography," Phys. Med. Biol. **51**, R155-R167 (2006).